Bioactive Materials 27 (2023) 200–215

Contents lists available at ScienceDirect

Bioactive Materials

journal homepage: www.keaipublishing.com/en/journals/bioactive-materials

In situ self-assembled organoid for osteochondral tissue regeneration with dual functional units

Zhen Yang [a,b,1], Bin Wang [c,1], Wei Liu [d], Xiaoke Li [e], Kaini Liang [f], Zejun Fan [f], Jiao Jiao Li [g], Yudi Niu [f], Zihao He [a,b], Hui Li [a,b], Du Wang [a,b], Jianjing Lin [h], Yanan Du [f,**], Jianhao Lin [a,b,***], Dan Xing [a,b,*]

[a] Arthritis Clinical and Research Center, Peking University People's Hospital, No.11 Xizhimen South Street, Beijing, 100044, China
[b] Arthritis Institute, Peking University, Beijing, 100044, China
[c] Department of Orthopedic Surgery, The First Affiliated Hospital, Zhejiang University School of Medicine, Hangzhou, 310006, China
[d] Beijing CytoNiche Biotechnology Co. Ltd, Beijing, 10081, China
[e] Department of Orthopedics, Shanxi Medical University Second Affiliated Hospital, Taiyuan, 030001, China
[f] Department of Biomedical Engineering, School of Medicine, Tsinghua-Peking Center for Life Sciences, Tsinghua University, Beijing, 10084, China
[g] School of Biomedical Engineering, Faculty of Engineering and IT, University of Technology Sydney, Sydney, Australia
[h] Department of Sports Medicine and Rehabilitation, Peking University Shenzhen Hospital, Shenzhen, China

ARTICLE INFO

Keywords:
Mesenchymal stem cells
Self-assembly
Microcryogels
Osteochondral regeneration
Organoid

ABSTRACT

The regeneration of hierarchical osteochondral units is challenging due to difficulties in inducing spatial, directional and controllable differentiation of mesenchymal stem cells (MSCs) into cartilage and bone compartments. Emerging organoid technology offers new opportunities for osteochondral regeneration. In this study, we developed gelatin-based microcryogels customized using hyaluronic acid (HA) and hydroxyapatite (HYP), respectively for inducing cartilage and bone regeneration (denoted as CH-Microcryogels and OS-Microcryogels) through *in vivo* self-assembly into osteochondral organoids. The customized microcryogels showed good cytocompatibility and induced chondrogenic and osteogenic differentiation of MSCs, while also demonstrating the ability to self-assemble into osteochondral organoids with no delamination in the biphasic cartilage-bone structure. Analysis by mRNA-seq showed that CH-Microcryogels promoted chondrogenic differentiation and inhibited inflammation, while OS-Microcryogels facilitated osteogenic differentiation and suppressed the immune response, by regulating specific signaling pathways. Finally, the *in vivo* engraftment of pre-differentiated customized microcryogels into canine osteochondral defects resulted in the spontaneous assembly of an osteochondral unit, inducing simultaneous regeneration of both articular cartilage and subchondral bone. In conclusion, this novel approach for generating self-assembling osteochondral organoids utilizing tailor-made microcryogels presents a highly promising avenue for advancing the field of tissue engineering.

1. Introduction

The osteochondral unit is composed of integrated layers of articular cartilage, calcified cartilage, and subchondral bone with a complex cartilage-bone interface and different properties among tissue layers [1]. A major scientific and clinical challenge remains to achieve simultaneous structural and functional repair of cartilage and subchondral bone in osteochondral injuries due to their dissimilar healing capacities and tissue integration properties, close interaction between cartilage and bone, and dynamic gradient changes along structural axes as well as different tissue development stages [2,3]. In attempts to mimic the hierarchical structure of the osteochondral unit, scaffolds with

Peer review under responsibility of KeAi Communications Co., Ltd.
* Corresponding author. Arthritis Clinical and Research Center, Peking University People's Hospital, No.11 Xizhimen South Street, Beijing, 100044, China.
** Corresponding author. Department of Biomedical Engineering, School of Medicine, Tsinghua-Peking Center for Life Sciences, Tsinghua University, Beijing, 10084, China.
*** Corresponding author. Arthritis Institute, Peking University, Beijing, 100044, China.
E-mail addresses: duyanan@tsinghua.edu.cn (Y. Du), linjianhao@pkuph.edu.cn (J. Lin), xingdan@bjmu.edu.cn (D. Xing).
[1] These authors contributed equally.

https://doi.org/10.1016/j.bioactmat.2023.04.002
Received 12 February 2023; Received in revised form 1 April 2023; Accepted 2 April 2023

biphasic, triphasic, multilayered and continuous gradient designs as well as anti-shear and anti-tensile properties have been developed, and achieved some degree of success in preclinical animal studies [2,4–8]. However, a number of limitations remain: (1) biphasic scaffolds typically fail to regenerate calcified cartilage and gradient tissue structure; (2) triphasic and multilayered scaffolds often exhibit substantial and abrupt changes between layers, which increase the chance of layer delamination and tissue separation under mechanical loading [5,9].

Self-assembled organoids have recently been developed for drug screening, mechanistic studies, and understanding organ development or tissue regeneration in a variety of organ systems such as the liver, kidney, brain, breast, taste buds, stomach and pancreas [10–12]. Excitingly, the development of multicellular organoids has emerged and may present a promising strategy for osteochondral regeneration [10]. Traditionally, the process of organoid self-assembly includes a series of cell differentiation processes and self-patterning that are highly modulated by multiple morphogenic agents, such as through 3D scaffolds with growth factor-conditioned media (including transforming growth factor-β (TGF-β), epidermal growth factor (EGF), fibroblast growth factor (FGF), and gastrin) [13]. These approaches provide some control over the organoid's biological characteristics, but current methods lack the ability to induce spatial patterning and developmental aspects of individual organoids through directional differentiation [14]. A primary limitation is that a single scaffold and specific media types are not sufficient for growing organoids with heterogeneous structures. Other methods have incorporated inductive growth factors into extracellular matrix (ECM)-mimicking fibers within MSC spheroids to induce the directional differentiation of MSCs [3]. However, the reliance on using growth factors presents limitations of high cost, easy inactivation and short half-life of growth factors, as well as reduced portability, injectability and long-term preservation of the resulting organoids [15].

Some recent studies aimed at osteochondral regeneration have attempted the construction of organoids with hierarchical structure. For example, Lee et al. used two kinds of composite spheroids consisting of adipose-derived MSCs and nanofibers incorporated with TGF-β3 and bone morphogenetic growth factor-2 (BMP-2) to form osteochondral units [3]. Interestingly, MSCs undergoing differentiation harvested from these osteochondral units were shown to mitigate carbon tetrachloride-induced mouse chronic liver fibrosis, suggesting a novel therapeutic strategy for *in vivo* organoid-derived cells in disease treatment. To create the zonal structures of osteochondral tissue, genetically distinct subpopulations of cartilaginous tissue were developed into organoids and used as living building blocks to mimic the native developmental process, and achieved *in vivo* assembly into a dual structure of cartilage and subchondral bone [16]. Such approaches of assembling functional tissue building blocks introduce new avenues for producing biomimetic scaffolds with zone-specific functionality.

As we previously reported, injectable microcryogels could provide a 3D microenvironment for loading matrices, cells and bioactive factors to create tailored cellular niches for tissue repair in various experimental models, including disc degeneration, liver cirrhosis, wound healing and limb ischemia [17–21]. In addition, we showed that MSC-laden microcryogels could undergo self-assembly to form 3D functional tissue constructs, which increased MSC stemness and paracrine activity while reducing MSC senescence [22]. The idea of using porous microcryogels as scaffolding to create osteochondral organoids presents the advantages of providing: (1) good cytocompatibility; (2) large specific surface area to enhance cell growth; and (3) convenient interactions with molecules and drugs [23]. To further improve the chondrogenic phenotype of cells within MSC-laden microcryogels, a chemical cross-linking strategy can be considered [24].

In the present study, we developed an *in situ* self-assembled organoid for osteochondral regeneration that presents hierarchical tissue structure without reliance on a bulk scaffold or use of growth factors. First, we designed and constructed hyaluronic acid (HA)- and hydroxyapatite (HYP)-modified gelatin-based microcryogels, which were respectively denoted CH-Microcryogels (for chondrogenic differentiation) and OS-Microcryogels (for osteogenic differentiation). Then, MSCs were preloaded onto these customized microcryogels and underwent chondrogenic or osteogenic pre-differentiation induction for 7 d before *in vitro* or *in vivo* self-assembly by sequential injection to form integrated bone and cartilage layers. mRNA-seq conducted on pre-differentiated customized microcryogels revealed the mechanisms of directional chondrogenic and osteogenic differentiation of MSCs in the microcryogels. Sequential injection of pre-differentiated customized microcryogels into osteochondral defects in beagle dogs achieved *in situ* self-assembly into osteochondral organoids and substantial *in vivo* tissue repair in the absence of other inducing factors, suggesting the usefulness of this approach as a simplistic, injectable solution for the regeneration of complex interfacial tissue.

2. Materials and methods

2.1. Study design

A schematic of the study design is shown in Fig. 1. To provide a suitable microenvironment for MSC chondrogenic and osteogenic differentiation, hyaluronic acid (HA) and hydroxyapatite (HYP) were respectively added into the gelation-based precursor solution to form CH-Microcryogels and OS-Microcryogels after freezing, planking, washing, and lyophilization. MSCs were seeded into these customized CH-Microcryogels and OS-Microcryogels, followed by culturing in chondrogenic and osteogenic induction medium respectively for 7 d to form pre-differentiated cell-laden customized microcryogels. The pre-differentiated chondrogenic and osteogenic microcryogels were sequentially deposited in two layers to form osteochondral organoids by self-assembly. *In vitro* analyses were performed on both the osteochondral organoids and individual layers. Pre-differentiated osteogenic and chondrogenic microcryogels were then sequentially injected into osteochondral defects in the trochlear groove of beagle dogs. All knees were harvested for analysis at 3 and 6 months post-surgery. Undifferentiated MSC-laden microcryogels were used as the control group for *in vitro* and *in vivo* experiments.

2.2. Preparation and characterization of customized microcryogels

2.2.1. Fabrication of gelatin microcryogels

Gelatin microcytes were fabricated as we previously reported [21,22]. Briefly, a laser fabrication system (Rayjet) was used to prepare PMMA microstencil array chips, which contained 600 circular microwells (200 μm in diameter) treated using a plasma cleaner (Micro Technologies) to promote hydrophilicity. The gelatin precursor solution (8% w/v gelatin) was prepared by dissolving gelatin in a water bath at 50 °C, followed by cooling in an ice bath for 10 min and adding 0.5% glutaraldehyde solution (100 μl) with gentle stirring. Aliquots of 250 μL precursor solution were injected evenly onto the upper surface of the PMMA chip, which was then stored at −20 °C for 16 h followed by lyophilization for 30 min (Boyikang). The lyophilized microgels were collected by a PMMA ejector pin array designed by a 3D milling machine (MDX-40 A; Roland DG), washed with 0.1 M $NaBH_4$ to remove unreacted aldehyde, and finally washed with distilled water 3 times. All microcryogels were collected, lyophilized and vacuum-packaged into a dish for subsequent experiments.

2.2.2. Fabrication of CH-Microcryogels and OS-Microcryogels

As shown in Table S1, the fabrication process of CH-Microcryogels and OS-Microcryogels was the same as for gelatin microcryogels, except that the precursor solutions were 8% gelatin +0.25% hyaluronic acid (w/v) and 8% gelatin +6% hydroxyapatite (w/v), respectively. To eliminate unreacted aldehyde residues, all microcryogels underwent a thorough washing procedure with 0.1 M $NaBH_4$. Subsequently, the microcryogels were subjected to a triple wash with distilled water to

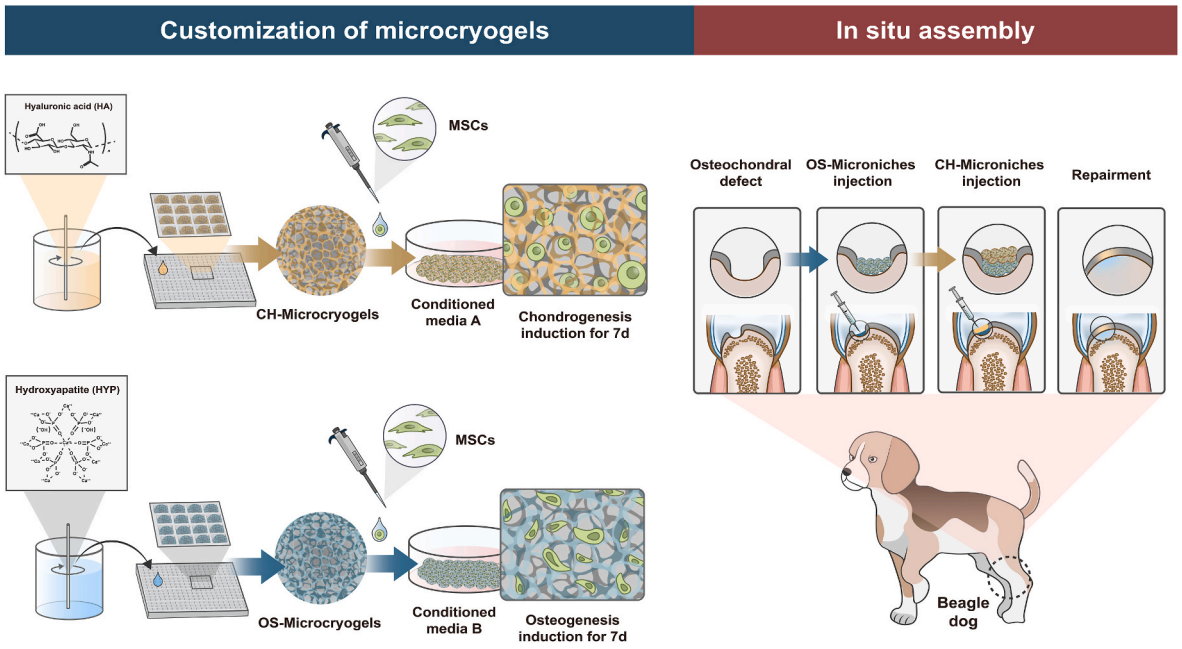

Fig. 1. Schematic diagram of the study design.

mitigate the deleterious effects of residual chemical groups on cell behavior.

2.2.3. Scanning electron microscopy (SEM) images

The microstructural properties of different microcryogels were characterized by SEM (FEI Quanta 200) after sputter coating with gold. Additionally, the diameter and aspect ratio of microcryogels were measured by the software Nano Measure1.2 (China) and ImageJ (USA), respectively.

2.2.4. Water absorption

The water absorption capacity of different microcryogels was measured by weighing the freeze-dried and swollen constructs according to a previous study [25]. Briefly, dry microcryogels were weighed [W_0] and then rehydrated in distilled water at 37 °C for 24 h to reach the equilibrium swelling state. Then, wet microcryogels were removed from the distilled water and weighed [W_1]. The water uptake rate was calculated according to the following equation:

$$Q = [(W_1–W_0)/W_0] \times 100\%$$

2.3. Preparation of MSC-laden microcryogels

2.3.1. Cell culture and seeding

Human umbilical cord MSCs were acquired from EUBIO Technologies and cultured in MSC growth medium (BioWit Technologies), as previously described [22]. Before cell seeding, the lyophilized microcryogels were sterilized by ethylene oxide (AN74j/Anprolene; Anderson Sterilization). A cell suspension containing 2.5×10^6 cells suspended in 200 μl DMEM culture medium (low glucose, Corning, USA) was seeded onto 20 mg microcryogels evenly distributed in a cell culture dish (40 mm in diameter), followed by immediate incubation in a humidified chamber for 2 h (37 °C, 5% CO_2) to ensure cell adhesion [19]. Finally, fresh culture medium (low glucose DMEM+10% FBS+1% Penicillin-Streptomycin Solution) was added to allow cell proliferation in microcryogels.

2.3.2. Live/dead staining

To confirm the viability of cells seeded on microcryogels, live/dead staining was performed after 7 d of culture. Briefly, the cultured microcryogels were gently washed with fresh PBS buffer and immersed in 1 mL of PBS working solution with 1 mM calcein-AM and 2 mM ethidium homodimer-1 for 30 min at room temperature. Excitation wavelengths of 556 nm and 488 nm were used on a Leica TCS-SP8 confocal microscope (Leica, Germany) to visualize calcein-AM (green color for live cells) and ethidium homodimer-1 (red color for dead cells).

2.3.3. SEM images

The microstructure of the MSC-seeded microcryogels was observed by SEM. Cultured microcryogels were harvested at 7 d after MSC seeding. After serial dehydration, the samples were sputter coated with gold, and images were obtained using SEM (Hitachi, Tokyo, Japan).

2.4. Chondrogenic and osteogenic pre-differentiation induction of MSC-seeded customized microcryogels

2.4.1. Differentiation induction

MSCs were seeded onto CH-Microcryogels and OS-Microcryogels. After cell adhesion, chondrogenic (Cyagen Biosciences, HUXUC-90041) and osteogenic (Cyagen Biosciences, HUXUC-90021) induction medium were respectively used to induce cell differentiation according to the manufacturer's instructions. After 7 d of culture, the cells were digested and collected for further analysis.

2.4.2. Histological staining

To investigate the differentiation-inducing effects of customized microcryogels on MSCs, the cells were harvested after 7 d of chondrogenic or osteogenic induction, seeded on 2D culture flask and cultured overnight. The samples undergoing chondrogenic differentiation were washed with PBS three times before toluidine blue (Solarbio, China) and safranin O staining (Solarbio, China), and samples undergoing osteogenic differentiation were stained with Alizarin red (Solarbio, China). Staining results were visualized by an Olympus optical microscope.

2.4.3. Alkaline phosphatase (ALP) quantitative detection

ALP staining as an indicator of osteogenesis was performed as previously reported [26]. Briefly, a total of 5×10^5 cells harvested from

control microcryogels and OS-Microcryogels were washed and fixed, and ALP staining was performed with the BCIP/NBT alkaline phosphatase color development kit (Beyotime, China) according to the manufacturer's instructions.

2.4.4. Quantitative RT–PCR

Total RNA was extracted from MSCs grown in microcryogels using the TRIzol reagent (Invitrogen, USA), and reverse transcription to cDNA was performed using a ReverTra Ace qPCR RT Kit (FSQ-201; TOYOBO). RT-PCR was performed using a CFX96 Real-Time System (Bio-Rad), with gene primers as listed in Table S2. Gene expression was evaluated relative to the housekeeping gene (GAPDH) by the comparative Ct ($2^{-\Delta\Delta CT}$) method. Three independent assays were conducted for each group.

2.4.5. Micromechanical testing

After 7 d of culture, atomic force microscopy (AFM, module Cohesion® 200 JPK, Instruments) was used to investigate the micromechanical compression properties of different microcryogels, as previously reported [22]. Before detection, the microcryogels were collected and frozen in liquid nitrogen for 1 h, dried and vacuum-packaged for 30 h, and evenly placed on a glass slide. The ARROW-TL1-50 silicon tipless cantilever (NANOWORLD), which was used to indent the samples, possessed a nominal spring constant of 0.03 N/m and was attached with a 6-μm length silicon microsphere on the cutting edge. For each sample, more than 25 different indentation locations were detected with up to ~2 nN force at a 5 μm/s displacement rate. Finally, the load–displacement curve was fitted to the Hertz model to acquire the effective indentation modulus.

2.4.6. F-actin/DAPI staining

The cytoskeleton of differentiated MSCs in microcryogels was analyzed by staining with F-actin (Beyotime Biotechnology, China) and 4',6-diamidino-2-phenylindole (DAPI, Beyotime Biotechnology, China). After washing the microcryogels two times with fresh PBS, the samples were observed by a TCS-SP8 STED 3X confocal microscope (Leica, Germany).

2.5. Self-assembly and characterization of osteochondral organoids

2.5.1. Osteochondral organoid self-assembly

Before organoid self-assembly from MSC-laden customized microcryogels, meshed frames (7 × 7 × 4 mm) were designed by AUTOCAD software (Autodesk Inc) and printed in PLA using a 3D printer (AOD printer Inc), as previously reported [22]. The space of meshes was no more than 100 μm to prevent overflow of microcryogels. Fabricated meshes were sterilized by immersion in 75% ethanol for 12 h and then rinsed three times with PBS solution, followed by UV irradiation for 30 min. Subsequently, MSC-laden OS-Microcryogels were pipetted as a bottom layer in the meshed frame, followed by pipetting CH-Microcryogels as a top layer. The composite was transferred to osteochondral induction medium, which is a combination of chondrogenic and osteogenic induction medium (Cyagen Biosciences) at 1:1 (v:v). The medium was refreshed at 3 d over 7 d of culture.

2.5.2. SEM images of self-assembled osteochondral organoids

The microstructure of self-assembled osteochondral organoids was visualized by SEM. Briefly, organoids were harvested after 14 d of culture in osteochondral induction medium, followed by fixation in PBS solution (pH: 7.4) with 2.5% (w/v) glutaraldehyde. After serial dehydration, the samples were sputter coated with gold, and images were obtained using SEM (Hitachi, Tokyo, Japan).

2.5.3. Cell-tracker analysis

Cell tracker was used to distinguish cells and investigate cell behavior in different microcryogels. Before cell seeding, the cells were incubated with 1x dye prepared in Diluent C provided in the kit (Sigma-Aldrich, MO, USA) according to the manufacturer's instructions. MSCs were labeled with PKH26 Red Fluorescent Cell Linker (for CH-Microcryogels) and MSCs with PKH67 Green Fluorescent Cell Linker (for OS-Microcryogels). The labeled cells were then seeded into different microcryogels and cultured according to the procedures in section 2.5.1 for self-assembly. Assembled organoids were imaged using a TCS-SP8 confocal microscope (Leica, Germany) at 490 nm (PKH67) and 551 nm (PKH26) excitation wavelengths.

2.5.4. Live/dead staining of osteochondral organoids

Live/dead staining was performed to confirm cell viability within osteochondral organoids. The organoids were gently washed with fresh PBS buffer and immersed in 1 mL of PBS working solution with 1 mM calcein-AM and 2 mM ethidium homodimer-1 for 30 min at room temperature. Excitation wavelengths of 556 nm and 488 nm were used on a Leica TCS-SP8 confocal microscope (Leica, Germany) to visualize calcein-AM (green color for live cells) and ethidium homodimer-1 (red color for dead cells).

2.5.5. Quantitative RT–PCR of osteochondral organoids

To confirm directional chondrogenic and osteogenic differentiation within assembled organoids, the cells were harvested from separated parts of the organoid incised in the axial position, followed by total RNA extraction. The expression of chondrogenic and osteogenic genes were detected by RT–PCR, as described in section 2.4.2.

2.5.6. Subcutaneous implantation in nude rats

To confirm biocompatibility and the ability of assembled organoids to maintain directional chondrogenic and osteogenic differentiation *in vivo*, the organoids were subcutaneously implanted into the back skin of nude rats. At 7 d post-implantation, the rats were euthanized, and the samples were harvested followed by H&E staining.

2.5.7. AFM of osteochondral organoids

AFM was used to investigate the micromechanical compression properties of osteochondral organoids, as previously reported [22]. Before detection, the organoids were collected and frozen in liquid nitrogen for 1 h, dried and vacuum-packaged for 30 h, and evenly on a glass slide. Micromechanical testing was performed as described in 2.4.5.

2.6. mRNA-seq analysis of osteochondral organoids

Human umbilical cord MSCs at passage 4 were seeded on CH-Microcryogels and OS-Microcryogels, and chondrogenic or osteogenic induction was conducted for 7 d according to procedures in 2.4.1. Control microcryogels were also subjected to chondrogenic and osteogenic induction over the same time period. After 7 d of induction culture, the samples were harvested at Shanghai Biotechnology Corporation (Shanghai, China) and prepared for mRNA-seq analysis [27]. Next-generation sequencing (NGS) technology using a high-throughput sequencer (Illumina NovaSeq6000) was used to sequence cDNA. The RNeasy Micro kit (Cat# 74,004, Qiagen) was used to extract total RNA, which was purified by the RNAclean XP Kit (Cat A63987, Beckman Coulter, Inc. Kraemer Boulevard Brea, CA, USA) and RNase-Free DNase Set (Cat# 79,254, QIAGEN, GmBH, Germany). After the sequence library was constructed, the purified total RNA was separated, fragmented, synthesized to cDNA, and 3' end added and ligated. Qubit®2.0 Fluorometer and Agilent 4200 system were chosen to detect and quantify all libraries. After the p-value was evaluated and the raw reads were stored in fastq format, the fold changes and significance of differences were determined. The differentially expressed genes (DEGs) with fold changes greater than 1.5 or less than 0.67 and p-values less than 0.05 were defined as significantly different. Each group included three independent biological replicates.

2.7. In vivo experiment

2.7.1. Surgical procedures

All animal experiments were conducted according to the Institutional Animal Care and Use Committee at Peking University Peoples' Hospital. Six healthy adult Beagle dogs (male, 6 months, weight 20 ± 5 kg) were used to evaluate *in vivo* repair by osteochondral organoids by creating osteochondral defect in the femoral condyle. At each time point, three dogs were randomly allocated into each of three groups: (A) the negative control group, (B) the control microcryogel group (contained pre-differentiated MSCs), and (C) the *in situ* self-assembled osteochondral organoid group (contained pre-differentiated MSCs) (Fig. S6). After anesthesia, a trephine was used to create a critical osteochondral defect (5 mm in diameter and 3.5 mm in depth) on the medial femoral condyle. In the osteochondral organoid group, 50 μl of OS-Microcryogels suspension was first injected into the bottom of the defect, followed by 30 μl CH-Microcryogels suspension, and fibrin glue was finally sprayed to cover the defect. In the control microcryogel group, 80 μl of microcryogel suspension was injected into the defect, and the defect was sealed with fibrin glue. The negative control group received no treatment. The animals were euthanized for evaluation at 3 and 6 months post-surgery.

2.7.2. Gross observation

All explanted knee samples were photographed and observed by 3 independent evaluators (n = 3 knees per group for each time point). The defect infilling, macroscopic appearance and integration with host tissue at the border zone were evaluated blindly by 3 experts according to ICRS scoring system guidelines (Table S3) [28].

2.7.3. Magnetic resonance imaging (MRI) analysis

All explanted knees underwent MRI analysis using a volume coil on a laboratory small animal-designed MRI scanner (BioSpec70/20USR, Bruke, Germany). T2-weighted spin−echo images with fat suppression were obtained in the sagittal planes. After the images were acquired, data were transferred and analyzed on a standalone computer. WORMS scoring assessment of the fat-suppressed T2-weighted MRI images was performed (Table S4).

2.7.4. Histological analysis

Following the above analyses, all samples were fixed in 4% (w/v) polyformaldehyde (PFA) for 72 h and decalcified in 10% (w/v) ethylenediaminetetraacetic acid (EDTA) for 3 months at room temperature. Samples were then dehydrated and embedded in paraffin, and sectioned into 5-μm slices along the coronal face. Hematoxylin and eosin (H&E), safranin O/fast green, and Masson staining were applied to detect osteochondral regeneration using light microscopy. Three independent images were also blindly scored by experienced researchers according to the modified O'Driscoll score system [29].

2.8. Statistical analysis

All quantitative data were analyzed using SPSS version 18.0 (Chicago, IL, USA) and expressed as mean ± standard deviation (SD). Student's *t*-test and one-way analysis of variance (one-way ANOVA), followed by the Bonferroni multiple comparison test, were performed for normally distributed data. A value of $P < 0.05$ was considered to indicate a statistically significant difference.

3. Results

3.1. Preparation and characterization of customized microcryogels

The fabrication process of customized microcryogels is shown in Fig. 2A, and the detailed compositions of customized microcryogels are shown in Table S1. Microcryogels were subjected to macroscopic and SEM evaluation after fabrication. All microcryogel groups had porous structures, with control microcryogels and CH-Microcryogels showing larger pores than OS-Microcyrogels (Fig. 2B). The average diameters of control microcryogels, CH-Microcryogels and OS-Microcryogels were 175.39 ± 50.64 μm, 217.10 ± 68.35 μm, and 98.16 ± 29.94 μm, respectively (Fig. 2C). Water absorption measurements showed that the control microcryogels had the highest water absorption (19.13-fold), followed by CH-Microcryogels (14.85-fold) and OS-Microcryogels (6.82-fold) (Fig. 2D). The three groups showed no significant differences in aspect ratio measurements (0.6282, 0.6659 and 0.6576) (Fig. 2E). Live/dead staining with calcein AM/PI and quantitative analysis indicated good cytocompatibility of all microcryogels. The presence of some red fluorescence in CH-Microcryogels and OS-Microcryogels may be attributed to non-specific dye binding to the materials. (Fig. 2F and G). The micromorphology of MSCs on different microcryogels was analyzed by SEM, where the MSCs were seen to spread out on the material surface and secrete ECM, while the microcryogels showed certain degradation and morphological changes (Fig. 2H). As shown in Fig. S1, the CH-Microcryogels floated on the surface of PBS solution, while OS-Microcryogels sank to the bottom, potentially attributable to dissimilarities in density and structure between the two types of microcryogels.

3.2. Chondrogenic and osteogenic differentiation in customized microcryogels before self-assembly

For evaluation of chondrogenic differentiation, MSCs seeded on control microcryogels and CH-Microcryogels underwent chondrogenic induction for 7 d (Fig. 3A). Toluidine blue and Alcian blue staining both indicated that CH-Microcryogels induced stronger chondrogenic differentiation than control microcryogels (Fig. 3B). CH-Microcryogels also showed significantly higher relative gene expression of COL2 and SOX9, although no difference was noted in ACAN expression (Fig. 3C–E). Interestingly, when compared with a 2D culture environment, CH-Microcryogels showed less osteogenic differentiation potential as indicated by Alizarin red staining and osteogenic differentiation-related gene expression (ALP, RUNX2, OCN and COL1) (Figs. S2E–I).

For evaluation of osteogenic differentiation, MSCs seeded on control microcryogels and OS-Microcryogels underwent osteogenic induction for 7 d (Fig. 3F). Alizarin red staining and quantitative detection of ALP both indicated that the OS-Microcryogels had stronger ability to promote osteogenic differentiation than control microcryogels (Fig. 3G–I). Interestingly, in a 2D culture environment, ALP activity in OS-Microcryogels was approximately 2-fold higher than in control microcryogels (Fig. 3I). OS-Microcryogels showed significantly higher expression of RUNX2 compared to control microcryogels, although no differences were noted in the expression of other osteogenic genes COL1, OCN and ALP (Fig. 3J-M). In addition, the OS-Microcryogels inhibited chondrogenic induction in MSCs when compared with a 2D culture environment (Figs. S2A–D).

The Young's modulus of customized microcryogels was measured by AFM after 7 d of chondrogenic and osteogenic induction (Fig. 3N and Fig. S2J). The average modulus of control microcryogels, CH-Microcryogels and OS-Microcryogels were 2.2, 4.5, and 7.3 kPa, respectively. F-actin staining was used to visualize the cytoskeleton of MSCs cultured in different microcryogels. The cytoskeleton in control microcryogels was thick, bunchy and neatly arranged, while cytoskeletal fibers in CH-Microcryogels were thinner, shorter, scattered in the cytoplasm, and non-directional (Fig. 3O). In comparison, fibers in the OS-Microcryogels were longer, thicker and more oriented than those in the control microcryogels (Fig. 3P).

3.3. Self-assembly of customized microcryogels into osteochondral organoids

As shown in Fig. 4A, the CH-Microcryogels and OS-Microcryogels were first subjected to 7 d of chondrogenic and osteogenic

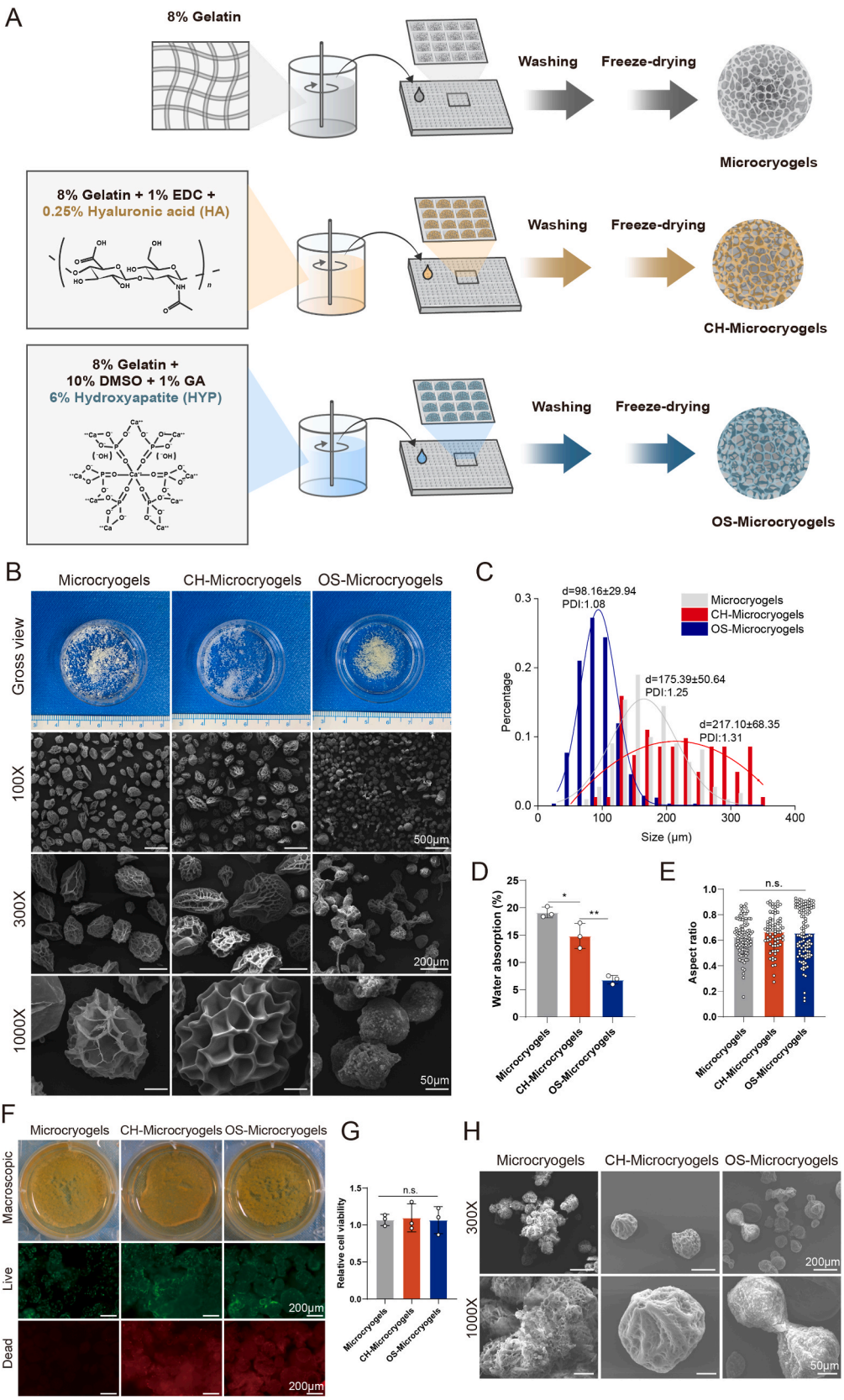

Fig. 2. Microscopic observation and cytocompatibility analysis of control microcryogels, CH-Microcryogels, and OS-Microcryogels. (A) Schematic of fabricating customized microcryogels. (B) Macroscopic view and SEM images of customized microcryogels at different magnifications (100X, 300X and 1000X). (C) Diameter distribution and polydispersity index (PDI) of customized microcryogels. (D) Water absorption rate of customized microcryogels. (E) Aspect ratio evaluation of customized microcryogels. (F) Macroscopic view and live/dead staining of MSCs cultured in customized microcryogels for 7 d. Representative 3D reconstruction images show live (green) cells and dead (red) cells. (G) Quantitative analysis of cell viability in customized microcryogels (n = 4). (H) SEM images of customized microcryogels after MSCs were seeded and grown for 14 d. (n.s. represents no significant difference).

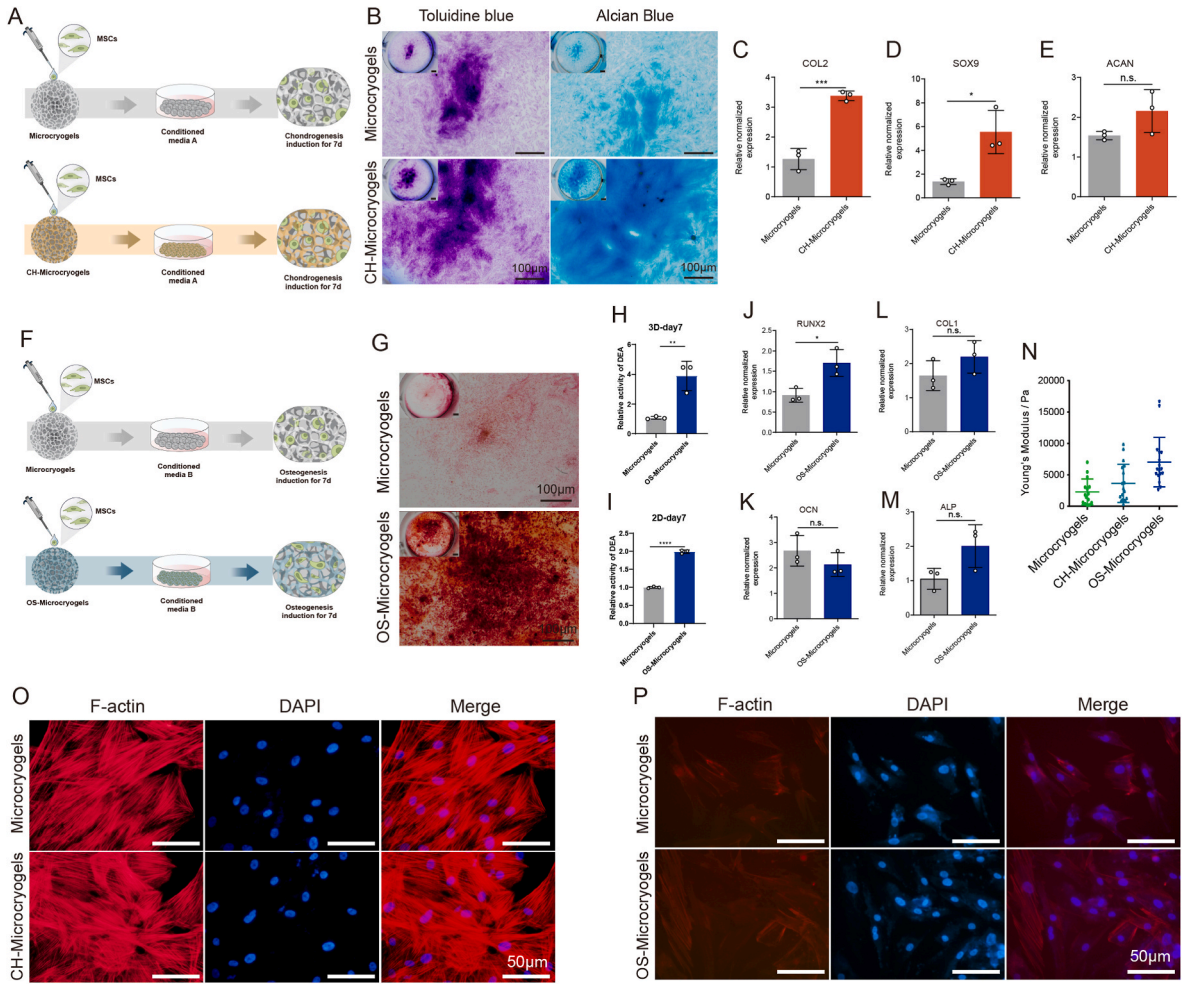

Fig. 3. *In vitro* chondrogenic and osteogenic pre-differentiation induction of MSC-seeded microcryogels. (A) Schematic of the chondrogenic induction process. (B) Toluidine blue and Alcian blue staining of control microcryogels and CH-Microcryogels after 7 d of chondrogenic induction. Relative gene expression of (C) COL2, (D) SOX9, and (E) ACAN. (F) Schematic of the osteogenic induction process. (G) Alizarin red staining of control microcryogels and OS-Microcryogels after 7 d of osteogenic induction. (H) Quantitative detection of ALP in MSCs after 7 d of osteogenic induction on control microcryogels and OS-Microcryogels. (I) Quantitative detection of ALP in MSCs on 2D culture plates. Relative gene expression of (J) RUNX2, (K) OCN, (L) COL1, and (M) ALP. (N) Atomic force microscopy (AFM) of microcryogels after 7 d of chondrogenic and osteogenic induction. F-actin and DAPI staining of MSCs cultured in microcryogels after 7 d of (O) chondrogenic induction and (P) osteogenic induction. (*$p < 0.05$, **$p < 0.01$, ***$p < 0.005$, n. s. represents no significant difference, $n = 3$).

differentiation induction, respectively. The pre-differentiated microcryogels were then pipetted into a 4 mm-length meshed frame, followed by 7 d of culture in mixed osteochondral induction medium (chondrogenic differentiation: osteogenic differentiation = 1:1). *In vitro* analyses were performed following self-assembly of pre-differentiated microcryogels into osteochondral organoid (Fig. 4A–C). Firstly, the osteochondral organoid was incised in the axial position to allow separate analysis of the chondrogenic and osteogenic components (supporting video 1). SEM imaging showed the microstructure of the osteochondral organoid, with a porous structure throughout and a well-integrated interfacial region between chondrogenic and osteogenic components (Fig. 4B–D). Cell tracking revealed that self-assembled organoids contained two layers of cells respectively located in CH-Microcryogels and OS-Microcryogels, where chondrogenic and osteogenic differentiation could be maintained and the two layers integrated well without blending into a mass of mixed cells (Fig. 4E). Live/dead staining of osteochondral organoids showed that almost all cells within CH-Microcryogels and OS-Microcryogels stayed alive after 14 d of induction (Fig. 4F). The presence of some red fluorescence in CH-Microcryogels and OS-Microcryogels may be attributed to non-specific dye binding to the materials. Osteochondral organoids were also incised in the middle, and the chondrogenic (CH-organoid) and osteogenic (OS-organoid) compartments were compared against non-assembled CH-Microcryogels and OS-Microcryogels. Interestingly, the gene expression of ACAN (2.5-fold), COL2 (5.05-fold), and SOX9 (1.71-fold) were all significantly higher in CH-organoids than CH-Microcryogels (Fig. 4G), while the expression of ALP (4.69-fold), RUNX2 (2.34-fold), and OCN (2.27-fold) were significantly higher in OS-organoids compared to OS-Microcryogels (Fig. 4H).

To investigate *in vivo* biocompatibility, CH-Microcryogels and OS-Microcryogels were subcutaneously injected into nude rats. Histological analysis revealed no inflammatory infiltration. Interestingly, the two types of customized microcryogels had different ability to promote *in vivo* angiogenesis. Gross observation indicated no neovasculature in the CH-Microcryogels, while many blood vessels grew into the OS-Microcryogels (Fig. 4I). H&E staining further revealed the presence of neovascular tissue inside OS-Microcryogels but not CH-Microcryogels, suggesting that OS-Microcryogels had better potential to enhance vascularization (Fig. 4I, S5). The mechanical properties of the osteochondral organoids were evaluated by measuring the Young's modulus and comparing to its CH-organoid and OS-organoid components. The Young's modulus of the OS-organoid was significantly higher than the whole organoid and CH-organoid component (Fig. 4J and K).

Supplementary video related to this article can be found at https://

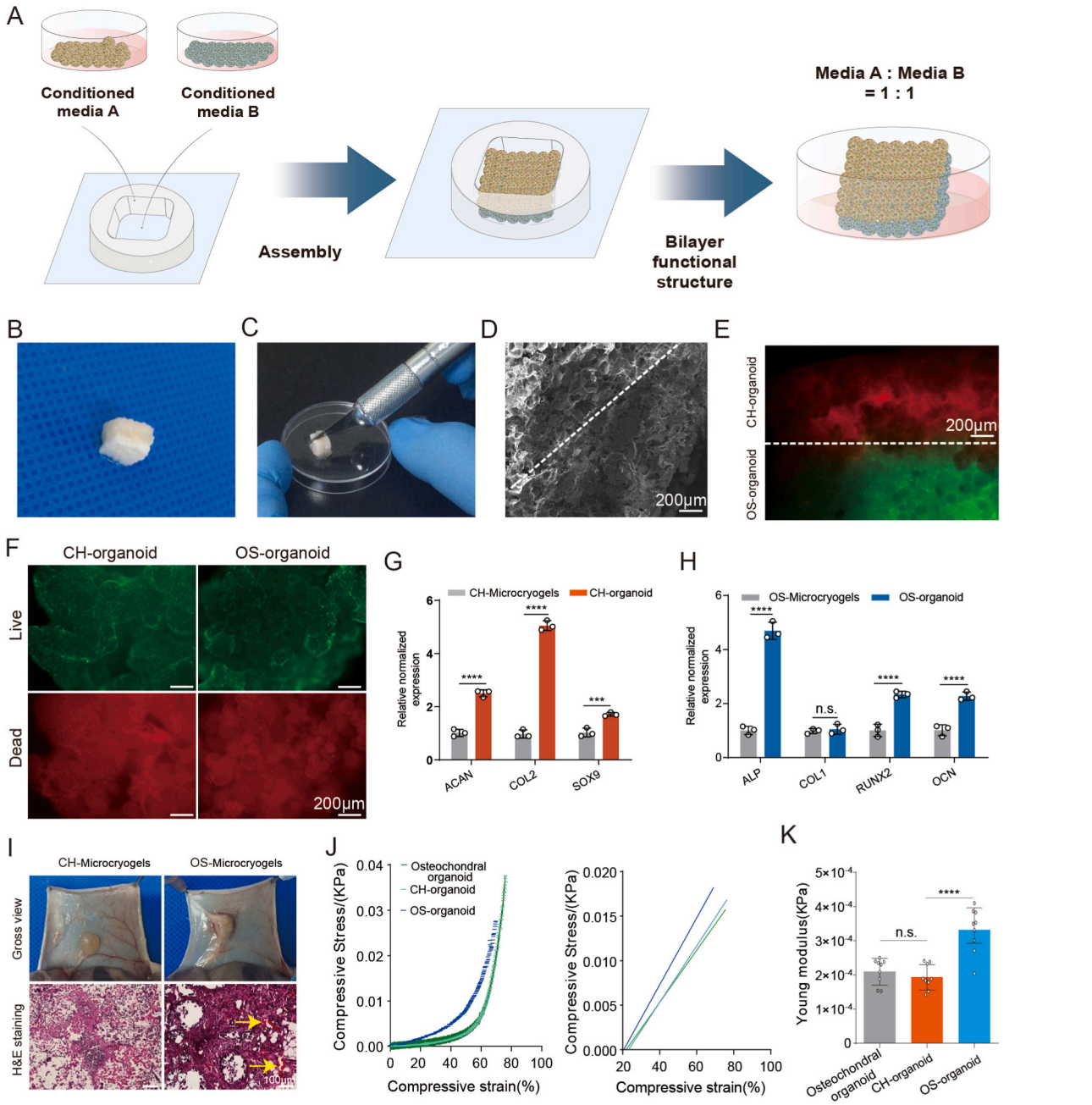

Fig. 4. *In vitro* self-assembly of osteochondral organoids over 14 d. (A) Schematic of *in vitro* self-assembly process of osteochondral organoids. (B) Gross observation of self-assembled osteochondral organoids. (C) The self-assembled osteochondral organoid was incised in the axial position to allow separate analysis of the chondrogenic and osteogenic components. (D) SEM image of self-assembled osteochondral organoids, showing the CH-Microcryogel part on the left of the dotted line and the OS-Microcryogel part on the right. (E) Cell tracking of self-assembled osteochondral organoids after 14 d of osteochondral induction. Red indicates MSCs in the CH-Microcryogel part, and green indicates MSCs in the OS-Microcryogel part. (F) Live/dead staining of the chondrogenic and osteogenic parts of self-assembled osteochondral organoids. (G) Relative chondrogenic gene expression of CH-Microcryogels and CH-organoids (chondrogenic part of osteochondral organoid). (H) Relative osteogenic gene expression of OS-Microcryogels and OS-organoids (osteogenic part of osteochondral organoid). (I) Macroscopic observations and H&E staining of CH-Microcryogels and OS-Microcryogels 1 week after subcutaneous implantation in nude rats (yellow arrows indicate new blood vessels). (J) Stress-strain curve of osteochondral organoid together with CH-organoid and OS-organoid components. (K) Young's modulus of osteochondral organoid together with CH-organoid and OS-organoid components.

doi.org/10.1016/j.bioactmat.2023.04.002

3.4. Customized microcryogels direct MSC fate

mRNA-seq analysis was performed on customized microcryogels to reveal the mechanisms by which they direct MSC fate. For chondrogenesis, MSCs grown in control microcryogels and CH-Microcryogels were compared after 7 d of chondrogenic induction (Fig. 5A). Principal component analysis (PCA) showed that all genes in the CH-Microcryogels group were highly distinct from those in the control microcryogels (Fig. S3A). A total of 4408 differentially expressed genes (DEGs, including 1615 downregulated genes and 2793 upregulated genes) were discovered (Fig. 5B and C). GO analysis showed significant enrichment of biological processes including regulation of mitotic cell cycle, cellular components including spindle, and molecular functions including protein serine/threonine/tyrosine kinase activity (Fig. S3B).

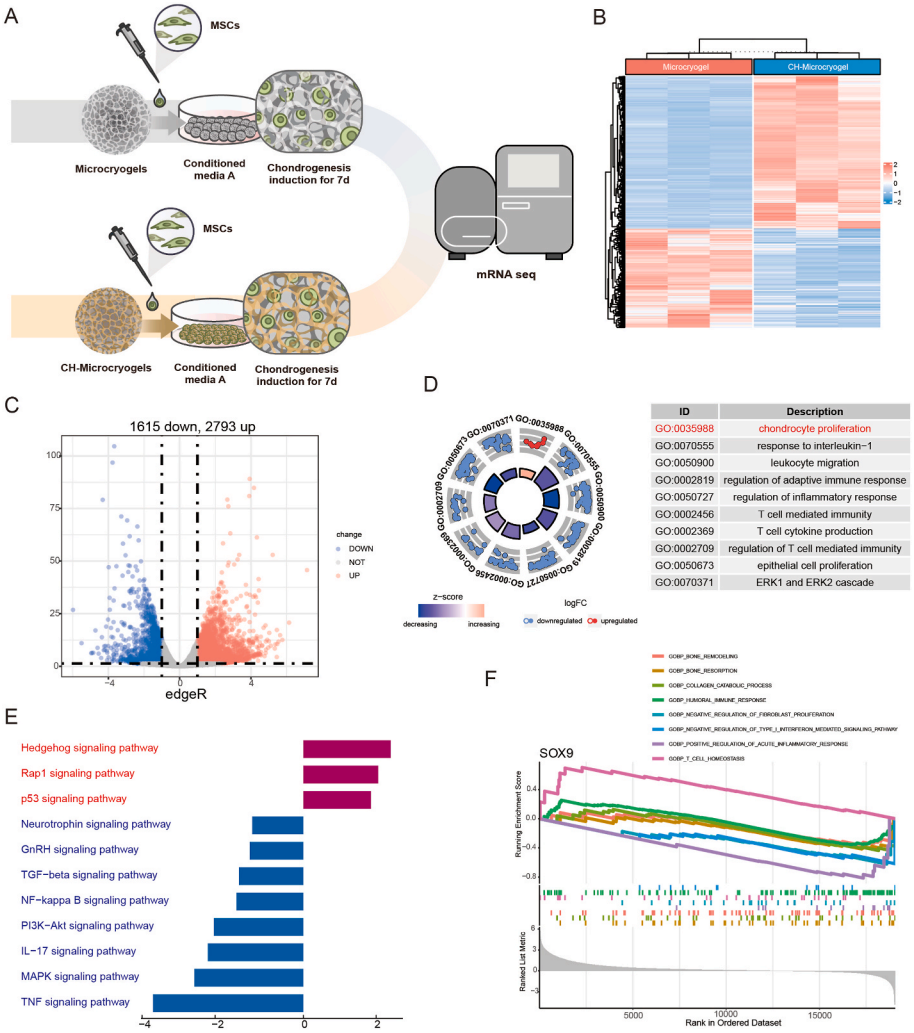

Fig. 5. mRNA-seq and DEG analyses of MSCs grown in control microcryogels and CH-Microcryogels after 7 d of chondrogenic induction. (A) Schematic of chondrogenic induction before mRNA-seq. (B) Heatmap distribution of control microcryogels and CH-Microcryogels. (C) Volcano diagram of control microcryogels and CH-Microcryogels (1615 downregulated DEGs, 2793 upregulated DEGs). (D) The significant GO of DEGs indicated that the effects of CH-Microcryogels on the regulation of MSCs were associated with chondrocyte proliferation and immunosuppression. (E) KEGG enrichment analysis of targeted genes indicated that the effects of CH-Microcryogels on the regulation of MSCs were associated with the hedgehog, rap1, TGF-β, PI3K-Akt, and MAPK signaling pathways. (F) GSEA of SOX9 in GO terms of bone remodeling, bone resorption, collagen catabolic process, humoral immune response, negative regulation of fibroblast proliferation, negative regulation of type I interferon mediated signaling pathway, positive regulation of acute inflammatory response, and T-cell homeostasis.

To better understand the GO functions of DEGs involved in cartilage regeneration, they were classified as: chondrocyte modulation and immune regulation. The GO term of chondrocyte proliferation was significantly upregulated, and immune response-related terms such as response to interleukin-1, leukocyte migration, regulation of inflammatory response, and T-cell-mediated immunity were downregulated (Fig. 5D). We also found DEGs related to chondrocyte proliferation (*Sox9*, *Mmp16*, and *Hmga2*), positive regulation of cell cycle processes (*Adam17, ddx11*, and *Cdca5*), and regulation of cell cycle G2/M phase transition (*Plk 1, Znf830,* and *Nabp1*) (Fig. S3C). In addition, the protein−protein interaction (PPI) network showed the connection of DEGs in different GO terms, especially the cell cycle G2/M phase transition and G2/M transition of the mitotic cell cycle (Fig. S3D). KEGG enrichment analysis of targeted genes showed 3 upregulated pathways, including the hedgehog, rap1, and p53 signaling pathways, and 8 downregulated pathways associated with immune regulation and chondrocyte hypertrophy, including the TGF-β, PI3K-Akt, and MAPK signaling pathways (Fig. 5E). We further explored the GSEA of SOX9 in GO terms and found that it was highly expressed in cell homeostasis and humoral immune response, but downregulated in bone remodeling, bone resorption, collagen catabolic process, negative regulation of fibroblast proliferation, negative regulation of type I interferon mediated signaling pathway, positive regulation of acute inflammatory response, and T-cell homeostasis (Fig. 5F).

For osteogenesis, MSCs grown in control microcryogels and OS-Microcryogels were compared after 7 days of osteogenic induction (Fig. 6A). A total of 2158 downregulated DEGs and 3213 upregulated DEGs were analyzed (Fig. 6B and C). GO analysis showed significant enrichment of biological processes including regulation of DNA metabolic process, cellular components including nuclear speck, and molecular functions including protein serine/threonine/tyrosine kinase activity (Fig. 6D, Fig. S4A). To further explore the regulatory mechanism of MSCs, we found 10 upregulated GO terms associated with osteoblast differentiation, ossification, bone development, bone growth, and bone mineralization (Fig. 6D). We analyzed the upregulated DEGs associated with bone development (*Col27a1, Bmp,* and *Foxn3*), ossification (*Runx2, Smad5,* and *Vcan*), positive regulation of osteoblast differentiation (*Bmp6, Bmpr2,* and *Runx2*), and the BMP signaling pathway (*Bmp6, Tgfb3,* and *Runx2*) (Figs. S4B–C). PPI analysis showed significant clustering in bone regeneration-related pathways, such as chondrocyte differentiation, cartilage development, and the TGF-β receptor signaling pathway (Fig. S4D). Interestingly, the KEGG analysis revealed that pathways associated with bone development (including PI3K-Akt, FoxO, TGF-β, MAPK, and Wnt signaling pathways) and immune modulation (mTOR, TNF, and IL-17 signaling pathways) were dramatically upregulated, while the apoptosis-related p53 signaling pathway was notably downregulated (Fig. 6E). We also discovered from the GSEA that COL1A was highly enriched in GO terms such as activation of MAPK activity, bone cell development, TGF-β production and vascular-associated smooth muscle contraction, but downregulated in GO terms such as positive regulation of macrophage migration and regulation of macrophage migration (Fig. 6F). RUNX2 was highly enriched in GO terms

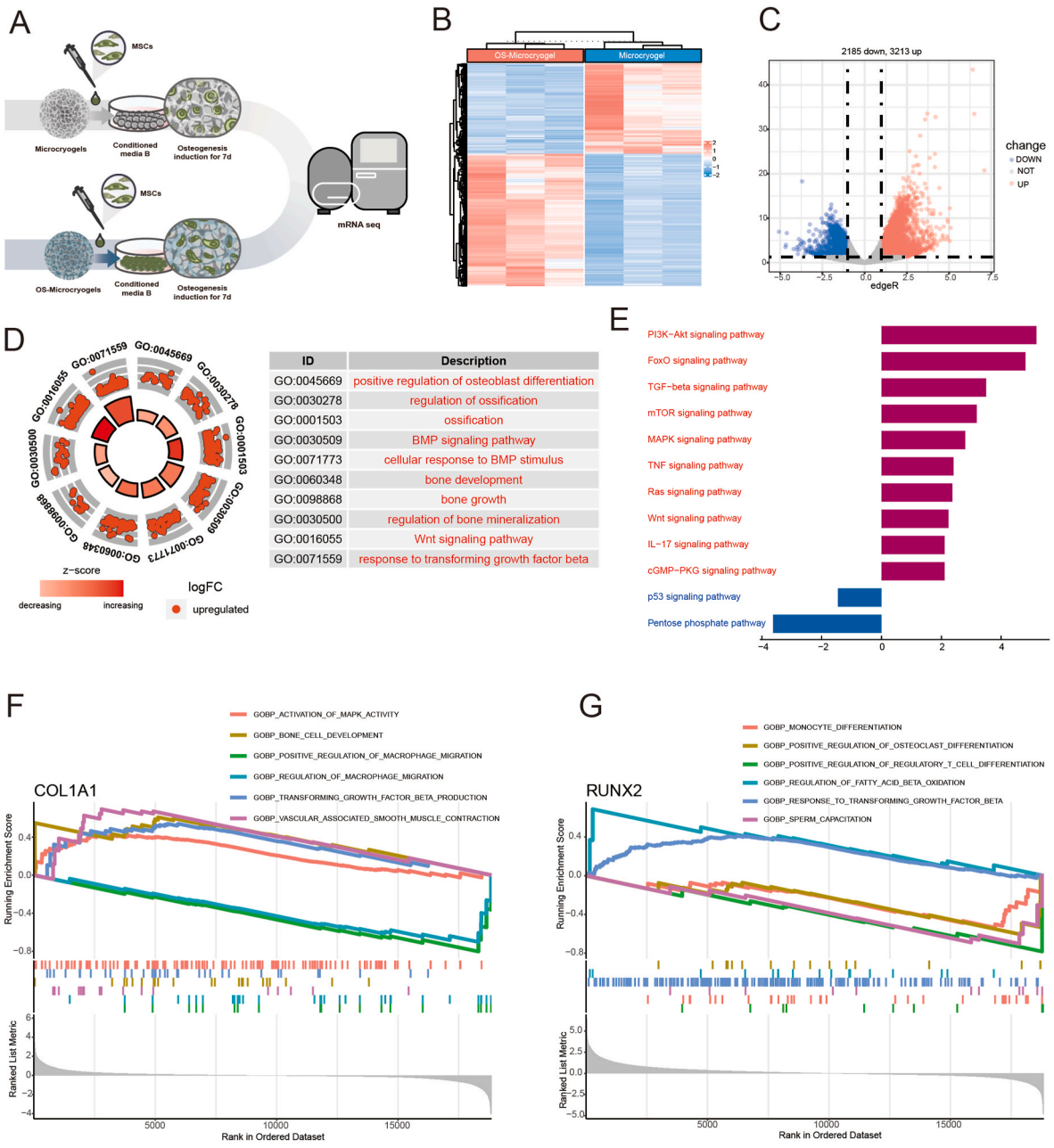

Fig. 6. mRNA-seq and DEG analyses of MSCs grown in control microcryogels and OS-Microcryogels after 7 d of osteogenic induction. (A) Schematic of osteogenic induction before mRNA-seq. (B) Heatmap distribution of control microcryogels and OS-Microcryogels. (C) Volcano diagram of control microcryogels and OS-Microcryogels (2185 downregulated DEGs, 3213 upregulated DEGs). (D) The significant GO of upregulated DEGs indicated that the effects of OS- Microcryogels on the regulation of MSCs were associated with osteoblast differentiation, ossification, bone development, bone growth, and bone mineralization. (E) KEGG enrichment analyses of targeted genes indicated that the effects of OS-Microcryogels on the regulation of MSCs were associated with the PI3K-Akt, FoxO, TGF-β, MAPK, and Wnt signaling pathways. (F) GSEA of COL1A1 in GO terms of activation of MAPK activity, bone cell development, positive regulation of macrophage migration, regulation of macrophage migration, transforming growth factor-beta production and vascular associated smooth muscle contraction. (G) GSEA of RUNX2 in the GO terms of positive regulation of osteoclast differentiation, response to transforming growth factor-beta, etc.

including regulation of fatty acid beta oxidation and response to TGF-β, but was downregulated in monocyte differentiation, positive regulation of osteoclast differentiation, and positive regulation of regulatory T-cell differentiation (Fig. 6G).

3.5. *Effect of self-assembled osteochondral organoids on treating in vivo osteochondral defects*

3.5.1. *MRI analysis*

The effects of osteochondral organoids formed by self-assembly from pre-differentiated customized microcryogels on treating osteochondral defects *in vivo* was tested using a beagle dog femoral trochlear defect model (Fig. 7A). The customized microcryogels were easily injected in sequential layers and fully filled the defect immediately upon injection, followed by *in situ* self-directed assembly into osteochondral organoids. Six months post-operation, the control group of beagle dogs displayed marked lameness, while the microcryogels treatment group showed visible improvements in gait albeit with mild residual lameness. Notably, the osteochondral organoid intervention group exhibited a normative gait (supporting video 2). MRI T2W1 sequence images

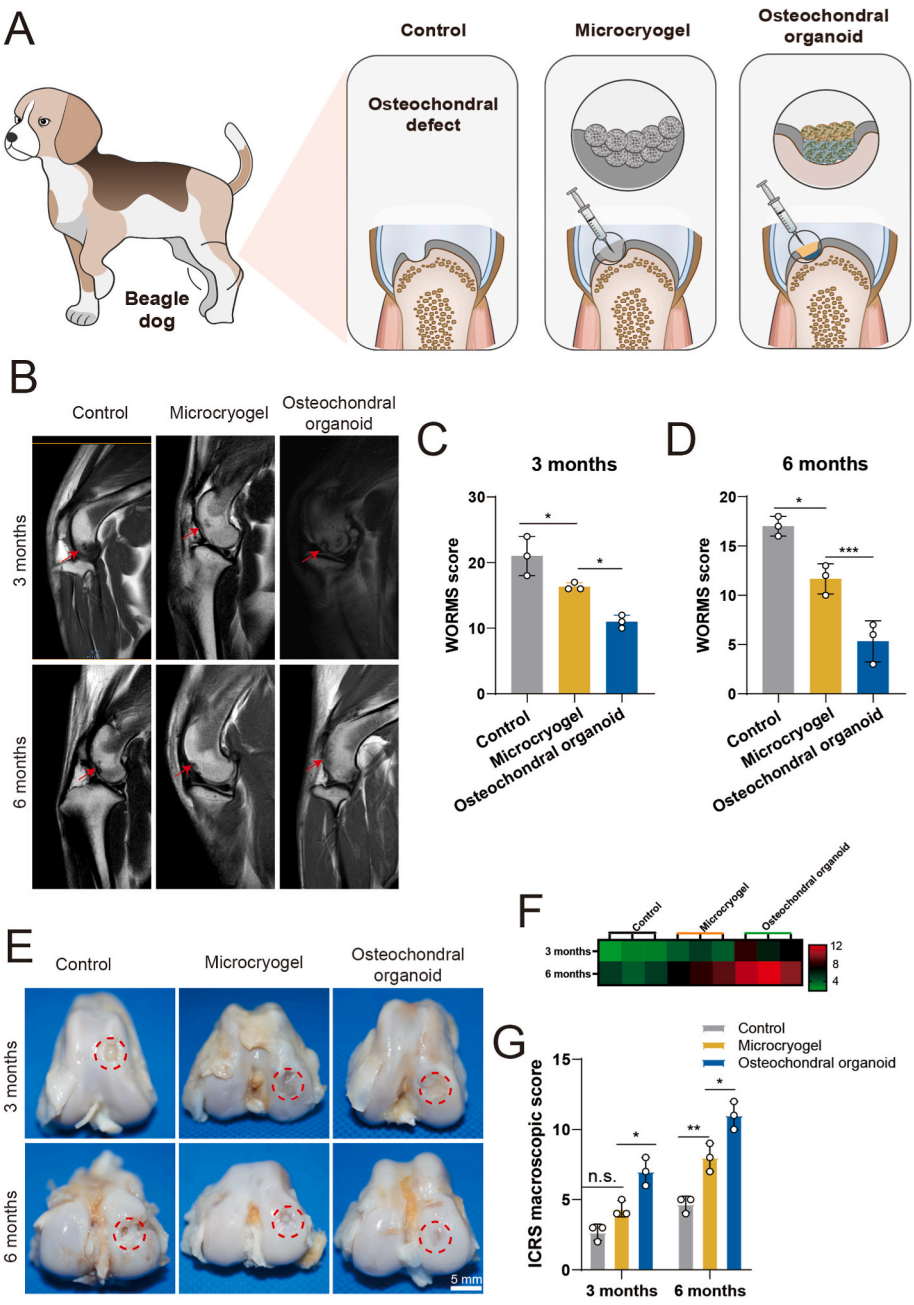

Fig. 7. *In vivo* analysis of osteochondral regeneration using *in situ* self-assembled organoids, including MRI and macroscopic evaluation of repair tissues. (A) Schematic of the *in vivo* experiment in beagle dogs. (B) MRI evaluation of the repair tissue at 3 and 6 months post-surgery. Red arrows indicate the region of repair tissue. (C, D) WORMS scoring of repair tissue at 3 and 6 months. (E) Macroscopic evaluation of repair tissue at 3 and 6 months. Red circles indicate the defect area. (F) Heatmap of ICRS macroscopic scores. (G) ICRS macroscopic scores of repair tissue at 3 and 6 months. (*p < 0.05, **p < 0.01, ***p < 0.005, n. s. represents no significant difference, n = 3).

indicate presence of repair tissue at 3 and 6 months (Fig. 7B). At 3 months post-surgery, all defect groups have not been completely filled with neotissue, and also showed some level of inflammation and edema in the subchondral bone. Compared with the untreated control group, a more continuous signal of the repaired tissue was observed in the control microcryogel and osteochondral organoid groups. At 12 months, edema of subchondral bone was still evident in the untreated control and control microcryogel groups, but had almost completely disappeared in osteochondral organoid group. In addition, the defect was completely filled only in the osteochondral organoid group, showing smooth and uniform repair tissue with a high level of similarity compared to the surrounding normal cartilage.

WORMS scoring for repaired knees indicated that the osteochondral organoid group achieved the best scores particularly at 6 months (3 months: 11.00 ± 1.00; 6 months: 5.33 ± 2.08), followed by the control microcryogel group (3 months: 16.33 ± 0.58; 6 months: 11.67 ± 1.53) and untreated control (3 months: 21.00 ± 3.00; 6 months: 17.00 ± 1.00) (Fig. 7C and D).

Supplementary video related to this article can be found at https://doi.org/10.1016/j.bioactmat.2023.04.002

3.5.2. *Macroscopic observation of repair tissue*

At 3 months, the macroscopic observation of repair tissue within the osteochondral defect suggested almost no cartilage-like tissue growth in the untreated control and control microcryogel groups, where defects were partly filled by granulation tissue that had a distinct surface from the surrounding cartilage (Fig. 7E). For the osteochondral organoid group, the defect showed much better coverage by repair tissue, although the appearance and flatness of the neotissue was still inferior to that of normal cartilage. At 6 months, untreated control defects were relatively smaller compared to at 3 months, and were covered with a few fibroblasts together with less subchondral bone exposure. In the control microcryogel group, the defect was mostly filled at 6 months although the repair tissue had a markedly irregular appearance. In the

osteochondral organoid group, the neotissue exhibited a consistent, glistening and smooth surface that was well integrated with surrounding cartilage without easily distinguishable borders.

The quality of repair tissue was evaluated by semiquantitative ICRS macroscopic scoring (Fig. 7F and G). The overall scores of repair tissues were presented in a heatmap, showing general improvement in all groups over time (Fig. 7F). At 3 months post-surgery, the ICRS macroscopic scores of the untreated control, control microcryogel, and osteochondral organoid groups were 2.67 ± 0.58, 4.33 ± 0.58, and 7.00 ± 1.00, respectively (Fig. 7G). At 6 months, the osteochondral organoid group achieved significantly higher scores (11.00 ± 1.00) than the other two groups (untreated control: 4.67 ± 0.58; control microcryogel: 8.00 ± 1.00).

3.5.3. *Histological evaluation of osteochondral defect repair*

Repair tissue in all groups was subjected to histological evaluation by H&E, safranin-O/fast green and Masson staining (Fig. 8). At 3 months, H&E staining indicated that the untreated control defect was poorly filled with evidence of abrasion and a blurred line between neotissue and surrounding normal cartilage and subchondral bone (Fig. 8A). Safranin-O/fast green staining also indicated the absence of a cartilage layer, and Masson staining revealed the structural disorder of bone trabeculae in the untreated control group. In the control microcryogel group, the defect showed better filling with neotissue, but with a very thin cartilage layer and disordered subchondral bone structure, as well as a clear boundary from the surrounding normal tissue. In contrast, the osteochondral organoid group showed a thicker cartilage layer with a smoother surface and better subchondral bone reconstruction. The modified O'Driscoll scores at 3 months confirmed that the osteochondral organoid group achieved better defect regeneration than the other two groups (Fig. 8B).

At 6 months, all groups exhibited improvement in tissue filling,

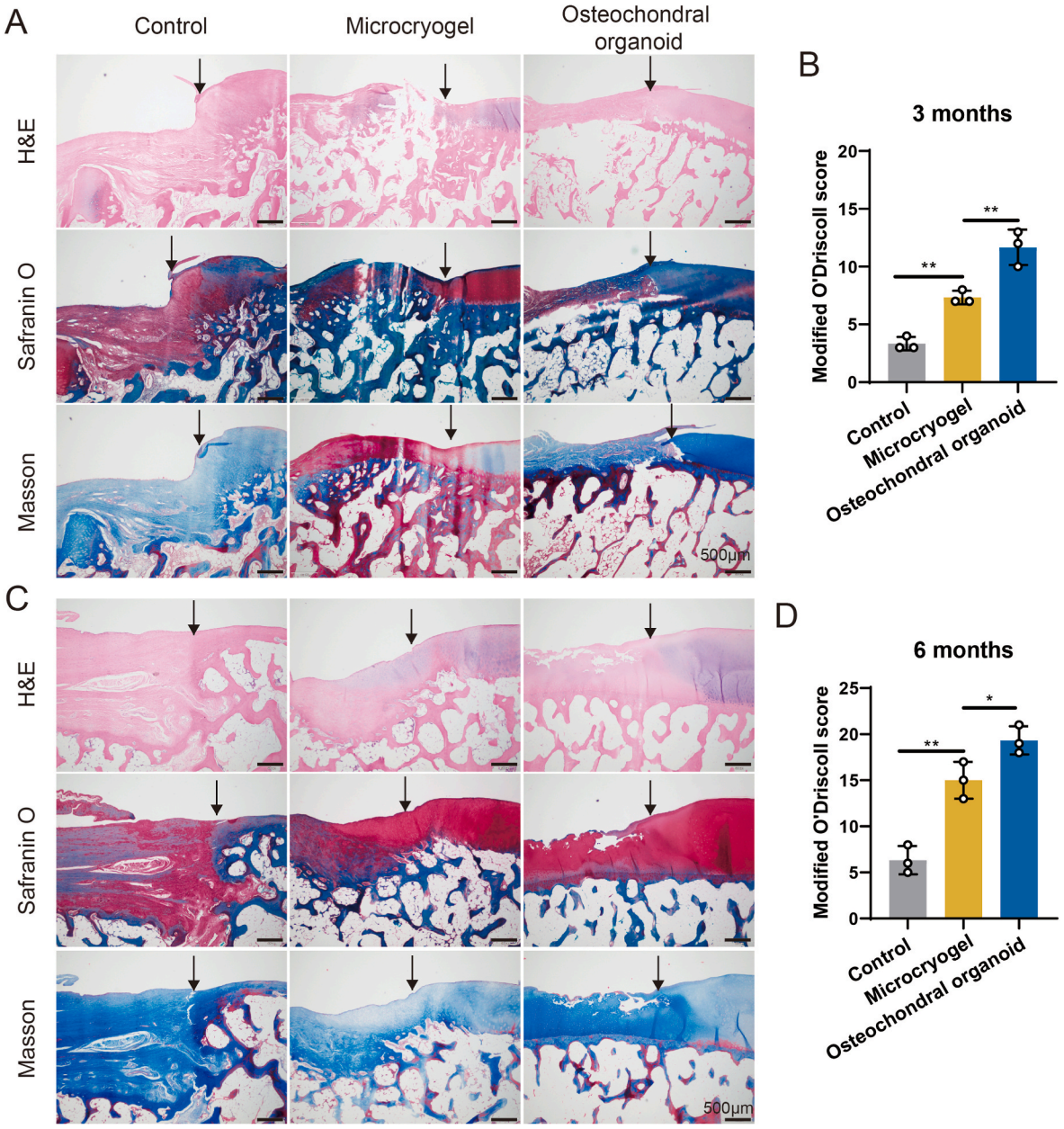

Fig. 8. Histological evaluation of repair tissue in osteochondral defects. (A, C) H&E, safranin O and Masson staining of repair tissue at 3 and 6 months post-surgery. Black solid arrows indicate the repair interface. (B, D) Modified O'Driscoll scores for histological evaluation of cartilage repair after 3 and 6 months (n = 3). (*$p < 0.05$, **$p < 0.01$).

boundary integration, surface smoothness of repair tissue, and subchondral bone reconstruction (Fig. 8C). In the untreated control group, the defect was filled with fibrous neotissue, showing severely damaged subchondral bone and poor boundary integration, which could not provide sufficient mechanical support. The control microcryogel group showed a thicker cartilage layer, but unsatisfactory reconstruction of subchondral bone. Promisingly, the neotissue in the osteochondral organoid group showed a more continuous hyaline cartilaginous structure with an even surface and satisfactory subchondral bone reconstruction. The modified O'Driscoll scores of the osteochondral organoid group remained significantly higher than the other two groups at 6 months (Fig. 8D).

4. Discussion

We developed a new strategy for constructing osteochondral organoid by mediating MSC directional differentiation through self-assembly of customized microcryogels. The microcryogels were customized by introducing HA into CH-Microcryogels to promote chondrogenic differentiation, and HYP into OS-Microcryogels to enhance osteogenic differentiation. These customized microcryogels presented excellent physical and biological microenvironments to direct MSC adhesion, proliferation and directional differentiation. We also found that compared to control microcryogels, the CH-Microcryogels could promote MSC chondrogenic differentiation by improving the secretion of glycosaminoglycan (GAG) and expression of chondrogenic genes. Meanwhile, the OS-Microcryogels enhanced MSC osteogenic differentiation as shown through increased calcium deposition, ALP activity, and RUNX2 gene expression. The functions of these customized microcryogels in inducing directional MSC differentiation have contributed to the construction of osteochondral organoid through self-assembly. Possible fate-directing mechanisms of customized microcryogels on MSCs were revealed by mRNA-seq, and bioinformatics analysis demonstrated regulation of chondrogenic and osteogenic differentiation processes as well as the modulation of inflammation and immune response. When the osteochondral organoids were implanted in canine femoral trochlear groove osteochondral defects, they achieved superior defect filling with neotissue and a biphasic cartilage-bone structure over 6 months compared to defects that were untreated or injected with control microcryogels. Collectively, these findings suggested that our self-assembled osteochondral organoids hold great promise as a simple and effective solution for osteochondral regeneration as well as for other interfacial tissue engineering applications.

In our previous studies, we developed cell-laden gelatin microcryogels which demonstrated the ability to induce ECM accumulation and self-assembly into micro-constructs, with strengthened cell-to-cell and cell-to-ECM interactions, creating a favorable microenvironment for driving long-term maintenance of MSC stemness, reduction of senescence and improvement of paracrine activity [22]. These self-assembled constructs were applied in cartilage repair and successfully achieved hyaline-like cartilage tissue regeneration in a rabbit femoral defect model [22]. In another study, self-assembled constructs loaded with undifferentiated and osteogenically induced MSCs in a ratio of 2:1 produced significant bone regeneration in a rat calvarial defect model [30]. These previous studies described cell-based therapeutic strategies using microcryogels for the individual repair of *in vivo* cartilage and bone defects. However, the simultaneous regeneration of structurally and functionally distinct cartilage and subchondral bone to form anatomically similar osteochondral tissue has not been attempted.

To address this challenge, we sought to create customized microcryogels by functionalizing standard microcryogels with additives to encourage the respective regeneration of cartilage and bone tissues. HA has been widely used in tissue engineering for loading MSCs or bioactive factors to modulate MSC fate, including adhesion, proliferation, phenotypic maintenance, antioxidant properties, or chondrogenic differentiation [31–34]. HYP is an inorganic mineral widely utilized in biomedical engineering, particularly for bone tissue regeneration and repair. Several studies have affirmed the role of HYP in mediating osteogenesis by MSCs, including by enhancing MSC adhesion, proliferation, and osteogenic differentiation by upregulating the expression of osteogenic markers such as alkaline phosphatase (ALP), osteocalcin (OCN), and bone sialoprotein (BSP) [35–38]. Additionally, HYP has been shown to activate key signaling pathways involved in osteogenic differentiation, including the bone morphogenetic protein (BMP) and Wnt signaling pathways [39–41]. HYP materials have also demonstrated strong osteogenic potential *in vivo*, both as scaffold-only and cell-seeded implants in a variety of small and large animal models of bone defects [35,42–46]. Moreover, HYP has been increasingly used for functionalizing scaffolds made from other materials to enhance osteogenic differentiation and suppress immunoinflammatory effects, since HYP can help provide a suitable microenvironment for MSC proliferation and differentiation [34,40,47,48]. Therefore, we chose HA and HYP respectively in this study to enhance the regulatory capacities of customized microcryogels on MSCs and direct them towards chondrogenic and osteogenic differentiation. As shown in Figs. 1–2, these customized microcryogels exhibited interconnected porous microstructures that provided a large surface area for efficient transportation of oxygen, nutrients, and waste products, thus promoting cell viability (Fig. 2) [22]. The diameters of CH-Microcyrogels and OS-Microcyrogels were 217.10 ± 68.35 μm and 98.16 ± 29.94 μm respectively, which were suitable for injection and cell delivery [49]. The pore size of CH-Microcyrogels was 50–100 μm, which could improve MSC infiltration and chondrocyte growth [49,50]. The water absorption rate of CH-Microcryogels was slightly lower than control microcryogels due to the addition of HA, while that of OS-Microcryogels was lower by more than two-thirds, which might have resulted from the higher molecular weight and lower solubility of HYP [51].

To enable *in situ* self-assembly of customized microcryogels into osteochondral organoid, the CH-Microcyrogels and OS-Microcyrogels were loaded with MSCs and subjected to chondrogenic and osteogenic pre-differentiation, respectively. For chondrogenic induction, biochemical stimulation with TGF-β was used to initiate the differentiation process. As seen in Fig. 3A and B, CH-Microcryogels loaded with MSCs and chondrogenically induced for 7 d exhibited stronger chondrogenic staining than control microcryogels, indicating that the addition of HA created a better microenvironment for MSC chondrogenic differentiation, as also shown in other studies [52]. This was also verified by significantly higher levels of chondrogenic gene expression (COL2 and SOX9) in CH-Microcryogels compared to control microcryogels (Fig. 3C–E). For osteogenic induction, OS-Microcryogels were customized by the addition of HYP (Fig. 3F). Following osteogenic induction for 7 d, the OS-Microcryogels showed enhanced ability to direct osteogenic differentiation of MSCs compared to control microcryogels, through staining and ALP detection (Fig. 3H and I) as well as early osteogenic gene expression (RUNX2) (Fig. 3J-M). A divergence was observed between ALP quantitative detection and ALP gene expression, which might have been due to the limitation of biological duplication of samples. The CH-Microcryogels and OS-Microcryogels demonstrated marked differences in various properties that might have helped direct differentiation outcomes. For instance, the OS-Microcryogels had much higher Young's modulus than the control microcryogels and CH-Microcryogels (Fig. 3N). Moreover, MSCs grown in CH-Microcryogels showed obvious differences in cytoskeletal structure and cell adhesion and extension compared to those grown in OS-Microcryogels (Fig. 3O-P). Gene expression results also indicated that OS-Microcryogels suppressed COL2 expression, while CH-Microcryogels suppressed ALP, RUNX2, OCN and COL1 expression, further confirming the ability of these customized microcryogels to differentially achieve chondrogenic and osteogenic conditioning of MSCs.

The CH-Microcryogels and OS-Microcryogels were deposited in sequential layers *in vitro* within a 3D printed frame to induce self-

assembly into osteochondral organoids, with the help of osteochondral induction medium (Fig. 4A). The organoids were seen to achieve layer integration through ECM secretion and microcryogel remodeling (Fig. 4B–D). During self-assembly, the CH-Microcryogels and OS-Microcryogels showed directional and zonal differentiation together with good maintenance of cell viability (Fig. 4E and F). Interestingly, MSCs in chondrogenic and osteogenic microcryogel layers after self-assembly into organoids showed stronger differentiation characteristics compared to those in individual customized microcryogels, as shown through gene expression analysis (Fig. 4G and H). In addition, the microcryogel layers within the organoid showed differing characteristics that were aligned with their functional purpose of maintaining chondrogenic or osteogenic differentiation, as seen through better vascular ingrowth (Fig. 4I) and higher Young's modulus (Fig. 4J and K) in the osteogenic layer compared to chondrogenic layer. These results suggested that the customized microcryogels were able to maintain ability to induce directional differentiation of MSCs following *in vitro* self-assembly into osteochondral organoids.

The results of mRNA-seq revealed some interesting insights into the mechanisms by which customized microcryogels direct MSC differentiation fate. For MSC chondrogenesis in CH-Microcryogels compared to control microcryogels, significant differences were observed in GO terms (Fig. 5). Notably, KEGG pathway analysis revealed that cell differentiation, migration and apoptosis-related pathways, including the hedgehog, Rap1, and p53 signaling pathways were significantly upregulated in CH-Microcryogels. Aligned with this, studies have found that transfection of the hedgehog gene into rabbit bone marrow-derived MSCs could enhance chondrogenic differentiation and inhibit cartilage aging under simulated microgravity [53], while blocking hedgehog signaling pathways by specific antagonists significantly decreased the chondrogenic capacity of MSCs [54]. Meanwhile, HMGB1 might promote the migration ability of MSCs through Rap1 pathway activation [55]. The CH-Microcryogels also showed significant downregulation of inflammation-related pathways, such as the neurotrophin, NF-κB, IL-17, and TNF signaling pathways, suggesting a more suitable microenvironment for inhibiting inflammation and immune activation [56]. The enhanced chondrogenic ability of CH-Microcryogels is supported by evidence suggesting that suppressing inflammation by selectively blocking the NF-κB signaling pathway could induce chondrogenesis [57], by attenuating the regulatory effect of TNF-α on stem cells [56]. Similarly, significant differences in osteogenesis-related GO terms were observed between MSCs subjected to osteogenic induction in OS-Microcryogels compared to control microcryogels (Fig. 6). Several osteogenesis-related pathways were significantly upregulated in OS-Microcryogels, including the PI3K-Akt, FoxO, TGF-β, MAPK, Wnt, and cGMP-pkg signaling pathways, while the cell apoptosis-related p53 signaling pathway was downregulated. Among these, the PI3K-Akt, TGF-β, and MAPK signaling pathways were found to be downregulated in CH-Microcryogels. Findings from a number of studies confirm the effects of regulating these signaling pathways on osteogenic differentiation. For instance, downregulation of TGF-β using matrine could inhibit Smad2/3-induced transcription and phosphorylation of ALP, OCN and RUNX2 after osteogenic induction [58]. The activation of MAPK pathways, such as through melatonin [59], could promote osteogenic transcription and matrix mineralization of MSCs [60–62] to enhance the efficiency of bone repair [59]. The differential regulation of PI3K-Akt activity in CH-Microcryogels and OS-Microcryogels is important for maintaining directional differentiation. PI3K-Akt signaling is required as a stage-dependent driver of chondrogenesis speed rather than hypertrophy, hence the inhibition of PI3K-Akt could reduce chondrocyte hypertrophy [63]. It also plays an important role in regulating osteogenic differentiation, as shown through a study that associated activation of the PI3K/Akt pathway with increased ALP activity, mineralization, and osteogenic gene expression (including β-catenin, osteocalcin and Runx2) [64]. These insights collectively highlight that the CH-Microcryogels and OS-Microcryogels could induce MSC directional differentiation by modulating the differential activation of the PI3K-Akt, TGF-β, and MAPK signaling pathways.

To evaluate the ability of the self-assembled osteochondral organoids in promoting *in vivo* osteochondral tissue regeneration, we injected pre-differentiated CH-Microcryogels and OS-Microcryogels as sequential layers into defects created in the femoral trochlear groove of beagle dogs (Figs. 7–8). These customized microcryogels formed osteochondral organoids by *in situ* self-assembly, likely by intensively interacting with host tissues and secreting regenerative proteins and cytokines within the defect site [65]. Considering the potential difficulties of maintaining the self-assembly process and maturation of newly formed cartilage and bone tissues without fixation, the injected layers of microcryogels were sealed by a fibrin glue cover. The *in vivo* results showed a significant inflammatory reaction in the joint cavity for the untreated control, where defects were poorly filled with loose fibrous tissue, which was consistent with observations that a deteriorating environment without protection would lead to failed regeneration [27,66]. Defects injected with control microcryogels exhibited a lower inflammatory reaction and better defect filling, but unsatisfactory histological osteochondral repair as evidenced by a thin cartilage layer and disordered subchondral bone, which is consistent with the results of other previous studies [67,68]. In comparison, the osteochondral organoid group achieved hierarchical regeneration of cartilage and bone within the osteochondral defect, showing seamless integration of both layers with surrounding native tissue as well as between the two layers. This approach of repairing osteochondral tissue through *in situ* self-assembly of injected layers of chondrogenic and osteogenic cell-ECM constructs is convenient and effective, which molds to the shape and size of the defect unlike bulk scaffolds, and is more practically applicable compared to growth factor-based approaches. Moreover, the microcryogels making up the organoid are highly porous and do not require physical or chemical cross-linking during cell seeding, thus significantly preserving cell viability and function *in vivo* [22]. To promote cartilage repair, TGF-β was added in a poly (lactic-co-glycolic acid)/gelatin scaffold to induce endogenous MSCs differentiation [67]. In addition, gelatin-based biphasic or triphasic scaffolds composited with MSCs or growth factors were also fabricated using 3D bioprinting or meltelectrowriting techniques and the *in vivo* osteochondral regeneration studies showed better effects than control defects [68–70]. However, the following concerns are still existing: complex preparation process, harsh material preservation conditions, and unsatisfactory effect of subchondral bone reconstruction. To addressed above problems, the approach for constructing osteochondral organoids by designing customized microcryogels was proposed in this study. Other potential approaches include the recent development of DNA nanostructures with excellent editability and biocompatibility for active drug delivery, tissue engineering, and biosensor development, which may help progress novel designs for osteochondral organoids [71–73].

The results of our study should be interpreted considering some limitations. Firstly, although we have identified molecular differences between the two types of customized microcryogels in regulating MSC differentiation, we have not investigated each specific molecular mechanism in detail. Further studies will focus on mechanism validation *in vitro* and *in vivo* through selective enhancement or inhibition of the identified pathways. Secondly, although we demonstrated promising *in vivo* osteochondral repair using a medium-sized animal model, the experiment was limited by a relatively small sample size and insufficient time to demonstrate full defect repair. Future work should explore longer term repair outcomes in large animals that more faithfully replicate human osteochondral anatomy and function. Thirdly, the animal model used in this study represented acute osteochondral injury and repair, while in humans the injury is often chronic with potential osteoarthritic changes. It would be of interest to investigate the effectiveness of repairing chronic osteochondral lesions using our osteochondral organoids and evaluate their ability in modulating the progression of trauma-induced joint disease. Fourthly, the *in vivo*

investigation has demonstrated that the osteochondral organoids exhibit superior performance in contrast to the microcryogels group. Nonetheless, their comparative efficacy against other prevailing treatment modalities remains uncertain. Consequently, it is imperative that we juxtapose our osteochondral organoids approach against clinically representative treatment methods in forthcoming investigations.

5. Conclusion

A novel approach was developed for constructing osteochondral organoids by designing customized microcryogels to differentially direct MSC fate. The gelatin-based microcryogels were modified by adding HA and HYP respectively to form customized CH-Microcryogels and OS-Microcryogels. These customized microcryogels showed good cytocompatibility and a powerful ability to differentially induce chondrogenic and osteogenic differentiation of MSCs. Following *in vitro* self-assembly of customized microcryogels, osteochondral organoids were successfully constructed without any delamination issues in the biphasic structure. mRNA-seq analysis revealed that the customized microcryogels directed MSC chondrogenic/osteogenic differentiation and regulated inflammation/immune-related pathways by modulating the PI3K-Akt, TGF-β, and MAPK signaling pathways. Finally, customized microcryogels injected sequentially *in vivo* led to *in situ* self-assembly into osteochondral organoids that achieved simultaneous regeneration of cartilage and subchondral bone in hierarchical layers. The present strategy of constructing self-assembled organoids using customized microcryogels has the potential to achieve effective regeneration of interfacial tissues without necessitating complex or demanding fabrication processes.

Declaration of competing interest

The authors declare that there are no conflicts of interest.

Ethics approval and consent to participate

All *in vivo* animal experiments were conducted according to the Institutional Animal Care and Use Committee at Peking University Peoples' Hospital.

CRediT authorship contribution statement

Zhen Yang: Data curation, Writing - original draft. **Bin Wang:** Conceptualization, Investigation. **Zejun Fan:** Methodology. **Yanan Du:** Conceptualization, Methodology, Resources. **Jianhao Lin:** Data curation, Funding acquisition, Supervision. **Dan Xing:** Conceptualization, Project administration, Supervision, Writing - review & editing.

Declaration of competing interest

The authors declare no competing interests.

Acknowledgments

This study was funded by grants from Beijing Natural Science Foundation (7212118, L222087) and Natural Science Foundation of China (81973606, 82272538). I would like to grant thanks to Beijing CytoNiche Biotechnology Co. Ltd, Beijing, China for assistance in developing microcryogels.

Appendix A. Supplementary data

Supplementary data to this article can be found online at https://doi.org/10.1016/j.bioactmat.2023.04.002.

References

[1] S. Ansari, S. Khorshidi, A. Karkhaneh, Engineering of gradient osteochondral tissue: from nature to lab, Acta Biomater. 87 (2019) 41–54.
[2] X. Niu, N. Li, Z. Du, X. Li, Integrated gradient tissue-engineered osteochondral scaffolds: challenges, current efforts and future perspectives, Bioact. Mater. 20 (2023) 574–597.
[3] J. Lee, S. Lee, S.J. Huh, B.J. Kang, H. Shin, Directed regeneration of osteochondral tissue by hierarchical assembly of spatially organized composite spheroids, Adv. Sci. 9 (3) (2022), e2103525.
[4] S.J. Seo, C. Mahapatra, R.K. Singh, J.C. Knowles, H.W. Kim, Strategies for osteochondral repair: focus on scaffolds, J. Tissue Eng. 5 (2014), 2041731414541850.
[5] B. Zhang, J. Huang, R.J. Narayan, Gradient scaffolds for osteochondral tissue engineering and regeneration, J. Mater. Chem. B 8 (36) (2020) 8149–8170.
[6] B. He, J.P. Wu, T.B. Kirk, J.A. Carrino, C. Xiang, J. Xu, High-resolution measurements of the multilayer ultra-structure of articular cartilage and their translational potential, Arthritis Res. Ther. 16 (2) (2014) 205.
[7] Y. Sun, Y. You, W. Jiang, B. Wang, Q. Wu, K. Dai, 3D bioprinting dual-factor releasing and gradient-structured constructs ready to implant for anisotropic cartilage regeneration, Sci. Adv. 6 (37) (2020).
[8] H. Da, S.J. Jia, G.L. Meng, J.H. Cheng, W. Zhou, Z. Xiong, Y.J. Mu, J. Liu, The impact of compact layer in biphasic scaffold on osteochondral tissue engineering, PLoS One 8 (1) (2013), e54838.
[9] L.M. Cross, A. Thakur, N.A. Jalili, M. Detamore, A.K. Gaharwar, Nanoengineered biomaterials for repair and regeneration of orthopedic tissue interfaces, Acta Biomater. 42 (2016) 2–17.
[10] S. Chen, X. Chen, Z. Geng, J. Su, The horizon of bone organoid: a perspective on construction and application, Bioact. Mater. 18 (2022) 15–25.
[11] K. Dai, Q. Zhang, S. Deng, Y. Yu, F. Zhu, S. Zhang, Y. Pan, D. Long, J. Wang, C. Liu, A BMP-2-triggered in vivo osteo-organoid for cell therapy, Sci. Adv. 9 (1) (2023), eadd1541.
[12] Y. Fang, R.M. Eglen, Three-Dimensional cell cultures in drug discovery and development, SLAS Discov 22 (5) (2017) 456–472.
[13] S. Rauth, S. Karmakar, S.K. Batra, M.P. Ponnusamy, Recent advances in organoid development and applications in disease modeling, Biochim. Biophys. Acta Rev. Canc 1875 (2) (2021), 188527.
[14] P. Hoang, Z. Ma, Biomaterial-guided stem cell organoid engineering for modeling development and diseases, Acta Biomater. 132 (2021) 23–36.
[15] Z. Yang, H. Li, Z. Yuan, L. Fu, S. Jiang, C. Gao, F. Wang, K. Zha, G. Tian, Z. Sun, B. Huang, F. Wei, F. Cao, X. Sui, J. Peng, S. Lu, W. Guo, S. Liu, Q. Guo, Endogenous cell recruitment strategy for articular cartilage regeneration, Acta Biomater. 114 (2020) 31–52.
[16] G.N. Hall, W.L. Tam, K.S. Andrikopoulos, L. Casas-Fraile, G.A. Voyiatzis, L. Geris, F.P. Luyten, I. Papantoniou, Patterned, organoid-based cartilaginous implants exhibit zone specific functionality forming osteochondral-like tissues in vivo, Biomaterials 273 (2021), 120820.
[17] Y. Zeng, C. Chen, W. Liu, Q. Fu, Z. Han, Y. Li, S. Feng, X. Li, C. Qi, J. Wu, D. Wang, C. Corbett, B.P. Chan, D. Ruan, Y. Du, Injectable microcryogels reinforced alginate encapsulation of mesenchymal stromal cells for leak-proof delivery and alleviation of canine disc degeneration, Biomaterials 59 (2015) 53–65.
[18] Y. Li, W. Liu, F. Liu, Y. Zeng, S. Zuo, S. Feng, C. Qi, B. Wang, X. Yan, A. Khademhosseini, J. Bai, Y. Du, Primed 3D injectable microniches enabling low-dosage cell therapy for critical limb ischemia, Proc. Natl. Acad. Sci. U. S. A. 111 (37) (2014) 13511–13516.
[19] C. Qi, Y. Li, P. Badger, H. Yu, Z. You, X. Yan, W. Liu, Y. Shi, T. Xia, J. Dong, C. Huang, Y. Du, Pathology-targeted cell delivery via injectable micro-scaffold capsule mediated by endogenous TGase, Biomaterials 126 (2017) 1–9.
[20] J. Wang, F. Chen, L. Liu, C. Qi, B. Wang, X. Yan, C. Huang, W. Hou, M.Q. Zhang, Y. Chen, Y. Du, Engineering EMT using 3D micro-scaffold to promote hepatic functions for drug hepatotoxicity evaluation, Biomaterials 91 (2016) 11–22.
[21] B. Wang, W. Liu, J.J. Li, S. Chai, D. Xing, H. Yu, Y. Zhang, W. Yan, Z. Xu, B. Zhao, Y. Du, Q. Jiang, A low dose cell therapy system for treating osteoarthritis: in vivo study and in vitro mechanistic investigations, Bioact. Mater. 7 (2022) 478–490.
[22] D. Xing, W. Liu, J.J. Li, L. Liu, A. Guo, B. Wang, H. Yu, Y. Zhao, Y. Chen, Z. You, C. Lyu, W. Li, A. Liu, Y. Du, J. Lin, Engineering 3D functional tissue constructs using self-assembling cell-laden microniches, Acta Biomater. 114 (2020) 170–182.
[23] D. Ghosh Dastidar, S. Saha, M. Chowdhury, Porous microspheres: synthesis, characterisation and applications in pharmaceutical & medical fields, Int. J. Pharm. 548 (1) (2018) 34–48.
[24] F. Li, C. Levinson, V.X. Truong, L.A. Laurent-Applegate, K. Maniura-Weber, H. Thissen, J.S. Forsythe, M. Zenobi-Wong, J.E. Frith, Microencapsulation improves chondrogenesis in vitro and cartilaginous matrix stability in vivo compared to bulk encapsulation, Biomater. Sci. 8 (6) (2020) 1711–1725.
[25] Z. Yuan, S. Liu, C. Hao, W. Guo, S. Gao, M. Wang, M. Chen, Z. Sun, Y. Xu, Y. Wang, J. Peng, M. Yuan, Q.Y. Guo, AMECM/DCB scaffold prompts successful total meniscus reconstruction in a rabbit total meniscectomy model, Biomaterials 111 (2016) 13–26.
[26] L. Zhao, L. Liu, Z. Wu, Y. Zhang, P.K. Chu, Effects of micropitted/nanotubular titania topographies on bone mesenchymal stem cell osteogenic differentiation, Biomaterials 33 (9) (2012) 2629–2641.
[27] Z. Yang, F. Cao, H. Li, S. He, T. Zhao, H. Deng, J. Li, Z. Sun, C. Hao, J. Xu, Q. Guo, S. Liu, W. Guo, Microenvironmentally optimized 3D-printed TGFβ-functionalized scaffolds facilitate endogenous cartilage regeneration in sheep, Acta Biomater. 150 (2022) 181–198.

[28] P. Mainil-Varlet, B. Van Damme, D. Nesic, G. Knutsen, R. Kandel, S. Roberts, A new histology scoring system for the assessment of the quality of human cartilage repair: ICRS II, Am. J. Sports Med. 38 (5) (2010) 880–890.
[29] Z. Yang, T. Zhao, C. Gao, F. Cao, H. Li, Z. Liao, L. Fu, P. Li, W. Chen, Z. Sun, S. Jiang, Z. Tian, G. Tian, K. Zha, T. Pan, X. Li, X. Sui, Z. Yuan, S. Liu, Q. Guo, 3D-Bioprinted difunctional scaffold for in situ cartilage regeneration based on aptamer-directed cell recruitment and growth factor-enhanced cell chondrogenesis, ACS Appl. Mater. Interfaces 13 (20) (2021) 23369–23383.
[30] H. Li, Z. He, W. Li, J.J. Li, J. Lin, D. Xing, Self-assembled microtissues loaded with osteogenic MSCs for in vivo bone regeneration, Front. Bioeng. Biotechnol. 10 (2022), 1069804.
[31] J. Yang, X. Wang, Y. Fan, X. Song, J. Wu, Z. Fu, T. Li, Y. Huang, Z. Tang, S. Meng, N. Liu, J. Chen, P. Liu, L. Yang, X. Gong, C. Chen, Tropoelastin improves adhesion and migration of intra-articular injected infrapatellar fat pad MSCs and reduces osteoarthritis progression, Bioact. Mater. 10 (2022) 443–459.
[32] G. Lisignoli, S. Cristino, A. Piacentini, S. Toneguzzi, F. Grassi, C. Cavallo, N. Zini, L. Solimando, N. Mario Maraldi, A. Facchini, Cellular and molecular events during chondrogenesis of human mesenchymal stromal cells grown in a three-dimensional hyaluronan based scaffold, Biomaterials 26 (28) (2005) 5677–5686.
[33] J. Hauptstein, T. Böck, M. Bartolf-Kopp, L. Forster, P. Stahlhut, A. Nadernezhad, G. Blahetek, A. Zernecke-Madsen, R. Detsch, T. Jüngst, J. Groll, J. Teßmar, T. Blunk, Hyaluronic acid-based bioink composition enabling 3D bioprinting and improving quality of deposited cartilaginous extracellular matrix, Adv Healthc Mater 9 (15) (2020), e2000737.
[34] W. Shi, F. Fang, Y. Kong, S.E. Greer, M. Kuss, B. Liu, W. Xue, X. Jiang, P. Lovell, A. M. Mohs, A.T. Dudley, T. Li, B. Duan, Dynamic hyaluronic acid hydrogel with covalent linked gelatin as an anti-oxidative bioink for cartilage tissue engineering, Biofabrication 14 (1) (2021).
[35] V. Hefka Blahnová, L. Vojtová, V. Pavliňáková, J. Muchová, E. Filová, Calcined hydroxyapatite with collagen I foam promotes human MSC osteogenic differentiation, Int. J. Mol. Sci. 23 (8) (2022).
[36] G. Calabrese, R. Giuffrida, C. Fabbi, E. Figallo, D. Lo Furno, R. Gulino, C. Colarossi, F. Fullone, R. Giuffrida, R. Parenti, L. Memeo, S. Forte, Collagen-hydroxyapatite scaffolds induce human adipose derived stem cells osteogenic differentiation in vitro, PLoS One 11 (3) (2016), e0151181.
[37] L.B. Jeng, H.Y. Chung, T.M. Lin, J.P. Chen, Y.L. Chen, Y.L. Lu, Y.J. Wang, S. C. Chang, Characterization and osteogenic effects of mesenchymal stem cells on microbeads composed of hydroxyapatite nanoparticles/reconstituted collagen, J. Biomed. Mater. Res. 91 (3) (2009) 886–893.
[38] S.I. Roohani-Esfahani, S. Nouri-Khorasani, Z. Lu, R. Appleyard, H. Zreiqat, The influence hydroxyapatite nanoparticle shape and size on the properties of biphasic calcium phosphate scaffolds coated with hydroxyapatite-PCL composites, Biomaterials 31 (21) (2010) 5498–5509.
[39] M.C. Lee, H. Seonwoo, K.J. Jang, S. Pandey, J. Lim, S. Park, J.E. Kim, Y.H. Choung, P. Garg, J.H. Chung, Development of novel gene carrier using modified nano hydroxyapatite derived from equine bone for osteogenic differentiation of dental pulp stem cells, Bioact. Mater. 6 (9) (2021) 2742–2751.
[40] Z. Zhong, X. Wu, Y. Wang, M. Li, Y. Li, X. Liu, X. Zhang, Z. Lan, J. Wang, Y. Du, S. Zhang, Zn/Sr dual ions-collagen co-assembly hydroxyapatite enhances bone regeneration through procedural osteo-immunomodulation and osteogenesis, Bioact. Mater. 10 (2022) 195–206.
[41] Y. Ramaswamy, I. Roohani, Y.J. No, G. Madafiglio, F. Chang, F. Zhang, Z. Lu, H. Zreiqat, Nature-inspired topographies on hydroxyapatite surfaces regulate stem cells behaviour, Bioact. Mater. 6 (4) (2021) 1107–1117.
[42] J. He, T. Huang, L. Gan, Z. Zhou, B. Jiang, Y. Wu, F. Wu, Z. Gu, Collagen-infiltrated porous hydroxyapatite coating and its osteogenic properties: in vitro and in vivo study, J. Biomed. Mater. Res. 100 (7) (2012) 1706–1715.
[43] H. Diao, Y. Si, A. Zhu, L. Ji, H. Shi, Surface modified nano-hydroxyapatite/poly (lactide acid) composite and its osteocyte compatibility, Mater Sci Eng C Mater Biol Appl 32 (7) (2012) 1796–1801.
[44] P. Guo, X. Liu, P. Zhang, Z. He, Z. Li, M. Alini, R.G. Richards, S. Grad, M. J. Stoddart, G. Zhou, X. Zou, D. Chan, W. Tian, D. Chen, M. Gao, Z. Zhou, S. Liu, A single-cell transcriptome of mesenchymal stromal cells to fabricate bioactive hydroxyapatite materials for bone regeneration, Bioact. Mater. 9 (2022) 281–298.
[45] L. Li, M. Yu, Y. Li, Q. Li, H. Yang, M. Zheng, Y. Han, D. Lu, S. Lu, L. Gui, Synergistic anti-inflammatory and osteogenic n-HA/resveratrol/chitosan composite microspheres for osteoporotic bone regeneration, Bioact. Mater. 6 (5) (2021) 1255–1266.
[46] Z. Zou, L. Wang, Z. Zhou, Q. Sun, D. Liu, Y. Chen, H. Hu, Y. Cai, S. Lin, Z. Yu, B. Tan, W. Guo, Z. Ling, X. Zou, Simultaneous incorporation of PTH(1-34) and nano-hydroxyapatite into Chitosan/Alginate Hydrogels for efficient bone regeneration, Bioact. Mater. 6 (6) (2021) 1839–1851.
[47] P. Zhang, X. Liu, P. Guo, X. Li, Z. He, Z. Li, M.J. Stoddart, S. Grad, W. Tian, D. Chen, X. Zou, Z. Zhou, S. Liu, Effect of cyclic mechanical loading on immunoinflammatory microenvironment in biofabricating hydroxyapatite scaffold for bone regeneration, Bioact. Mater. 6 (10) (2021) 3097–3108.
[48] G. Wang, Z. Lv, T. Wang, T. Hu, Y. Bian, Y. Yang, R. Liang, C. Tan, X. Weng, Surface functionalization of hydroxyapatite scaffolds with MgAlEu-LDH Nanosheets for high-performance bone regeneration, Adv. Sci. 10 (1) (2022), e2204234.
[49] W. Liu, Y. Li, Y. Zeng, X. Zhang, J. Wang, L. Xie, X. Li, Y. Du, Microcryogels as injectable 3-D cellular microniches for site-directed and augmented cell delivery, Acta Biomater. 10 (5) (2014) 1864–1875.
[50] S.H. Oh, I.K. Park, J.M. Kim, J.H. Lee, In vitro and in vivo characteristics of PCL scaffolds with pore size gradient fabricated by a centrifugation method, Biomaterials 28 (9) (2007) 1664–1671.
[51] J. Jeong, J.H. Kim, J.H. Shim, N.S. Hwang, C.Y. Heo, Bioactive calcium phosphate materials and applications in bone regeneration, Biomater. Res. 23 (2019) 4.
[52] A.K. Jha, W. Yang, C.B. Kirn-Safran, M.C. Farach-Carson, X. Jia, Perlecan domain I-conjugated, hyaluronic acid-based hydrogel particles for enhanced chondrogenic differentiation via BMP-2 release, Biomaterials 30 (36) (2009) 6964–6975.
[53] P.C. Liu, K. Liu, J.F. Liu, K. Xia, L.Y. Chen, X. Wu, Transfection of the IHH gene into rabbit BMSCs in a simulated microgravity environment promotes chondrogenic differentiation and inhibits cartilage aging, Oncotarget 7 (39) (2016) 62873–62885.
[54] X. Wu, Z.D. Cai, L.M. Lou, Z.R. Chen, The effects of inhibiting hedgehog signaling pathways by using specific antagonist cyclopamine on the chondrogenic differentiation of mesenchymal stem cells, Int. J. Mol. Sci. 14 (3) (2013) 5966–5977.
[55] F. Lin, D. Xue, T. Xie, Z. Pan, HMGB1 promotes cellular chemokine synthesis and potentiates mesenchymal stromal cell migration via Rap1 activation, Mol. Med. Rep. 14 (2) (2016) 1283–1289.
[56] R. Bi, K. Chen, Y. Wang, X. Luo, Q. Li, P. Li, Q. Yin, Y. Fan, S. Zhu, Regulating fibrocartilage stem cells via TNF-α/Nf-κB in TMJ osteoarthritis, J. Dent. Res. 101 (3) (2022) 312–322.
[57] T. Jiang, D. Kai, S. Liu, X. Huang, S. Heng, J. Zhao, B.Q.Y. Chan, X.J. Loh, Y. Zhu, C. Mao, L. Zheng, Mechanically cartilage-mimicking poly(PCL-PTHF urethane)/collagen nanofibers induce chondrogenesis by blocking NF-kappa B signaling pathway, Biomaterials 178 (2018) 281–292.
[58] D. Mao, X. Pan, Y. Rui, F. Li, Matrine attenuates heterotopic ossification by suppressing TGF-β induced mesenchymal stromal cell migration and osteogenic differentiation, Biomed. Pharmacother. 127 (2020), 110152.
[59] Y.H. Chan, K.N. Ho, Y.C. Lee, M.J. Chou, W.Z. Lew, H.M. Huang, P.C. Lai, S. W. Feng, Melatonin enhances osteogenic differentiation of dental pulp mesenchymal stem cells by regulating MAPK pathways and promotes the efficiency of bone regeneration in calvarial bone defects, Stem Cell Res. Ther. 13 (1) (2022) 73.
[60] D. Shao, M. Lu, D. Xu, X. Zheng, Y. Pan, Y. Song, J. Xu, M. Li, M. Zhang, J. Li, G. Chi, L. Chen, B. Yang, Carbon dots for tracking and promoting the osteogenic differentiation of mesenchymal stem cells, Biomater. Sci. 5 (9) (2017) 1820–1827.
[61] C. Xu, H. Liu, Y. He, Y. Li, X. He, Endothelial progenitor cells promote osteogenic differentiation in co-cultured with mesenchymal stem cells via the MAPK-dependent pathway, Stem Cell Res. Ther. 11 (1) (2020) 537.
[62] H. Niu, D. Lin, W. Tang, Y. Ma, B. Duan, Y. Yuan, C. Liu, Surface topography regulates osteogenic differentiation of MSCs via crosstalk between FAK/MAPK and ILK/β-Catenin pathways in a hierarchically porous environment, ACS Biomater. Sci. Eng. 3 (12) (2017) 3161–3175.
[63] F.A.M. Klampfleuthner, B. Lotz, T. Renkawitz, W. Richter, S. Diederichs, Stage-dependent activity and pro-chondrogenic function of PI3K/AKT during cartilage Neogenesis from mesenchymal stromal cells, Cells 11 (19) (2022).
[64] G.Y. Shen, H. Ren, J.J. Huang, Z.D. Zhang, W.H. Zhao, X. Yu, Q. Shang, T. Qiu, Y. Z. Zhang, J.J. Tang, D. Liang, Z.D. Yang, X.B. Jiang, Plastrum testudinis extracts promote BMSC proliferation and osteogenic differentiation by regulating let-7f-5p and the TNFR2/PI3K/AKT signaling pathway, Cell. Physiol. Biochem. 47 (6) (2018) 2307–2318.
[65] G.S. Kronemberger, R.A.M. Matsui, G. Miranda, J.M. Granjeiro, L.S. Baptista, Cartilage and bone tissue engineering using adipose stromal/stem cells spheroids as building blocks, World J. Stem Cell. 12 (2) (2020) 110–122.
[66] V. Church, T. Nohno, C. Linker, C. Marcelle, P. Francis-West, Wnt regulation of chondrocyte differentiation, J. Cell Sci. 115 (Pt 24) (2002) 4809–4818.
[67] Y. Han, B. Jia, M. Lian, B. Sun, Q. Wu, B. Sun, Z. Qiao, K. Dai, High-precision, gelatin-based, hybrid, bilayer scaffolds using melt electro-writing to repair cartilage injury, Bioact. Mater. 6 (7) (2021) 2173–2186.
[68] Y. Li, L. Li, Y. Li, L. Feng, B. Wang, M. Wang, H. Wang, M. Zhu, Y. Yang, E. I. Waldorff, N. Zhang, I. Viohl, S. Lin, L. Bian, W.Y. Lee, G. Li, Enhancing cartilage repair with optimized supramolecular hydrogel-based scaffold and pulsed electromagnetic field, Bioact. Mater. 22 (2023) 312–324.
[69] F. Gao, Z. Xu, Q. Liang, H. Li, L. Peng, M. Wu, X. Zhao, X. Cui, C. Ruan, W. Liu, Osteochondral regeneration with 3D-printed Biodegradable high-strength supramolecular polymer reinforced-gelatin hydrogel scaffolds, Adv. Sci. 6 (15) (2019), 1900867.
[70] Z. Qiao, M. Lian, Y. Han, B. Sun, X. Zhang, W. Jiang, H. Li, Y. Hao, K. Dai, Bioinspired stratified electrowritten fiber-reinforced hydrogel constructs with layer-specific induction capacity for functional osteochondral regeneration, Biomaterials 266 (2021), 120385.
[71] Y.W. Mei Zhang, Zhangheng Huang, Xin Qin, Mi Zhou, Dexuan Xiao, Weitong Cui, Zhiqiang Liu, Yunfeng Lin, Targeted therapy for autoimmune diseases based on multifunctional frame nucleic acid system_ Blocking TNF-α-NF-κB signaling and mediating macrophage polarization, Chem. Eng. J. 454 (2023).
[72] T. Tian, Y. Li, Y. Lin, Prospects and challenges of dynamic DNA nanostructures in biomedical applications, Bone Research 10 (1) (2022).
[73] Y. Gao, X. Chen, T. Tian, T. Zhang, S. Gao, X. Zhang, Y. Yao, Y. Lin, X. Cai, A lysosome-activated tetrahedral Nanobox for encapsulated siRNA delivery, Adv. Mater. 34 (46) (2022), e2201731.